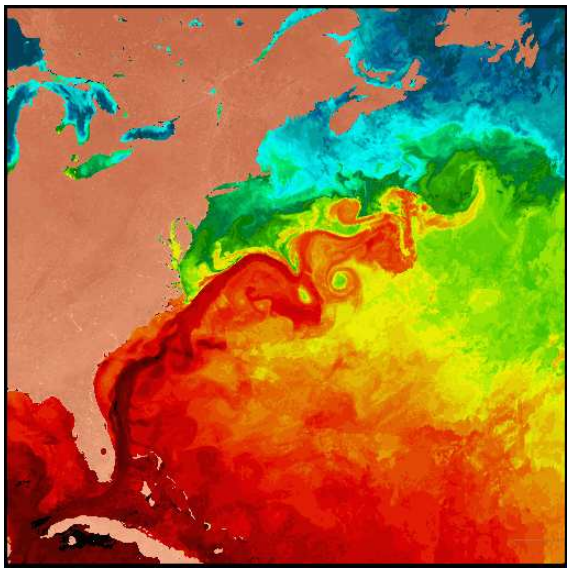

Large Scale Turbulence in the Atmosphere and Ocean

J. H. LaCasce

Dept. of Geosciences
University of Oslo
Oslo, Norway

LAST REVISED
12th May 2011

Joe LaCasce
Department for Geosciences
University of Oslo
P.O. Box 1022 Blindern
0315 Oslo, Norway
j.h.lacasce@geo.uio.no

Contents

1 Equations **4**
- 1.1 Basic equations . . . 4
- 1.2 Scaling . . . 7

2 Statistics in a nutshell **9**

3 The Fourier transform **12**

4 A chaotic example **14**

5 Conservation laws **22**
- 5.1 Energy . . . 22
- 5.2 Vorticity and enstrophy . . . 25

6 3-D turbulence **28**
- 6.1 Triad interactions . . . 28
- 6.2 Kolmogorov's inertial range . . . 31
- 6.3 Shell models . . . 35
- 6.4 Observations . . . 37

7 2-D turbulence **39**
- 7.1 A triad interaction . . . 41
- 7.2 An integral argument . . . 43
- 7.3 The two inertial ranges . . . 45
- 7.4 Physical interpretation . . . 49
- 7.5 The vortex view . . . 50
- 7.6 Passive tracer spectra . . . 56
- 7.7 Predictability . . . 59
  - 7.7.1 Lorenz Model . . . 60
  - 7.7.2 Predictability in 2-D turbulence . . . 61
  - 7.7.3 Predictability in the atmosphere . . . 63

8 Geostrophic turbulence **65**
- 8.1 The Beta-effect . . . 65
- 8.2 Beta turbulence in a closed basin . . . 73
- 8.3 Topography . . . 78
  - 8.3.1 The barotropic vorticity equation . . . 79
  - 8.3.2 Conserved quantities . . . 81
  - 8.3.3 Minimum enstrophy . . . 82
- 8.4 Stratification . . . 86
  - 8.4.1 Conserved quantities . . . 88
  - 8.4.2 Energy cascade . . . 90
  - 8.4.3 The vortex view . . . 92

8.4.4 Enstrophy cascade 94
8.4.5 Cascades in a two mode system 96

9 Turbulent Diffusion **104**
9.1 Single particle dispersion 105
9.1.1 Random walk 105
9.1.2 Diffusion 106
9.1.3 Single particle dispersion 108
9.1.4 The vortex merger problem 110
9.2 Two particle dispersion 114

1 Equations

1.1 Basic equations

To do what follows, we need to introduce the set of equations we'll be using, and the approximations we'll need. First are the momentum equations, written in vector form:

$$\frac{\partial}{\partial t}\vec{u} + \vec{u}\cdot\nabla\vec{u} + 2\Omega\times\vec{u} = -\frac{1}{\rho}\nabla p - g\hat{k} + \frac{1}{\rho}\frac{\partial}{\partial z}\vec{\tau} \tag{1}$$

Here $\vec{u}$ is the velocity, ρ is the density, p is the pressure, g is gravity, $\vec{\tau}$ is the applied stress and Ω is the rotation vector for the earth. Note that this equation is actually three equations in one—one for each spatial dimension.

We also have the continuity equation:

$$\frac{\partial}{\partial t}\rho + \vec{u}\cdot\nabla\rho + \rho(\nabla\cdot\vec{u}) = 0 \tag{2}$$

This expresses the conservation of mass. If the flux of density into a fixed volume is positive, the total mass will increase. Despite the simplicity of that idea, the equation is nonlinear and non-trivial.

But to simplify matters, we will make the *Boussinesq* approximation. This assumes that:

$$\rho = \rho_0 + \rho'(x, y, z, t) \tag{3}$$

where ρ_0 is a constant and that:

$$\rho_0 \gg |\rho'|$$

The density of water is nearly a constant—it changes only slightly when heated (over a reasonable range). So we can replace ρ in most of the equations by the constant ρ_0. This simplifies the continuity equation a lot:

$$\frac{\partial}{\partial t}\rho_0 + \vec{u} \cdot \nabla \rho_0 + \rho_0(\nabla \cdot \vec{u}) = 0 \tag{4}$$

or:

$$\nabla \cdot \vec{u} = 0 \tag{5}$$

Thus the Boussinesq fluid is *incompressible*. This means that volume is conserved.

The momentum equation is also simplified somewhat because the pressure term is now linear:

$$\frac{1}{\rho}\nabla p \quad \rightarrow \quad \frac{1}{\rho_0}\nabla p \tag{6}$$

The Boussinesq approximation is valid for the ocean and approximately so for the planetary boundary layer in the atmosphere. It is not accurate in the troposphere, due to the compressibility of air. But if one uses *pressure coordinates*, the pressure term is also linearized and the flow is incompressible. So the equations are similar to the Boussinesq ones we use hereafter.

We also require the stress term on the RHS of the momentum equation. We will write this as the sum of an (unspecified) forcing term and a diffusive damping term:

$$\frac{1}{\rho}\frac{\partial}{\partial z}\tau = \mathcal{F} + \nu \nabla^2 \vec{u} \tag{7}$$

The forcing could for example be the wind acting on the ocean, or convective motion in the atmosphere. The diffusion term represents molecular dissipation, with $\nu \approx 10^{-5}\ m^2/sec$.

We will alter the momentum equation slightly. For one, we can rewrite the advective term using incompressibility. Notice that:

$$\nabla \cdot (\vec{u}a) = \vec{u} \cdot \nabla a + a(\nabla \cdot \vec{u}) = \vec{u} \cdot \nabla a \tag{8}$$

Second, we can write the gravity term as the gradient of the *geopotential*, gz. Put together, we can write the momentum equation as:

$$\frac{\partial}{\partial t}\vec{u} + \nabla \cdot (\vec{u} \circ \vec{u}) + 2\Omega \times \vec{u} = -\nabla(\frac{p}{\rho_0} + gz) + \mathcal{F} + \nu\nabla^2\vec{u} \tag{9}$$

The circle in the advection term signifies a tensor product, because this actually represents 9 terms, in three separate equations. Thus the x-component is:

$$\frac{\partial}{\partial t}u + \nabla \cdot (\vec{u}u) - f_z v = -\frac{1}{\rho_0}\frac{\partial}{\partial x}p + F^x + \nu\nabla^2 u \tag{10}$$

where $f_z = 2\Omega sin(\theta)$ is the vertical component of the Coriolis acceleration (I'm ignoring the term involving the horizontal component, which is very small).

Interestingly, there is only one nonlinear term in this equation: the second term, the advection of momentum. This is a *quadratic* nonlinearity, because it involves the product of the unknown velocities. Turbulence springs from this term, as we'll see shortly.

1.2 Scaling

Not all the terms in the momentum equation are equally important. To see this, we approximate each of the terms with "typical" values, i.e. U, L, P, etc. The x-momentum equation scales as:

$$\frac{\partial}{\partial t}u + \nabla \cdot (\vec{u}u) - f_z v = -\frac{1}{\rho_0}\frac{\partial}{\partial x}p + F^x + \nu\nabla^2 u$$

$$\frac{U}{T} \qquad \frac{U^2}{L} \qquad fU \qquad \frac{P}{\rho_0 L} \qquad F \qquad \frac{\nu U}{L^2} \tag{11}$$

If we divide through by the last term, we get:

$$\frac{L^2}{\nu T} \qquad \frac{UL}{\nu} \qquad \frac{fL^2}{\nu} \qquad \frac{PL}{\rho_0 \nu U} \qquad \frac{FL^2}{\nu U} \qquad 1 \tag{12}$$

Thus the advection term is a factor of UL/ν times the size of the dissipation term. This parameter is the *Reynold's number*. How big is this? At the scale of weather systems in the atmosphere, we have:

$$\frac{UL}{\nu} \approx \frac{(10\,m/sec)(10^6\,m)}{10^{-5}\,m^2/sec} = 10^{12}$$

This means that advection is *much* more important than molecular dissipation at these scales.

The second point concerns the time scale, T. We can rewrite the first scaling term thus:

$$\frac{L^2}{\nu T} = \frac{T_\nu}{T} \tag{13}$$

This is the ratio between the actual time scale of the motion, T, and the *dissipation time scale*, $T_\nu = L^2/\nu$. This is the time scale approximately that is required for molecular friction to bring the motion at scale L to rest. How long is this? At the weather scales:

$$T_\nu = \frac{L^2}{\nu} \approx \frac{(10^6\, m)^2}{10^{-5}\, m^2/sec} = 10^{17}\ sec$$

This is roughly 10^{12} days, or about 3×10^9 years—roughly one fourth the age of the present universe! So we would have to wait for a very long time for molecular dissipation to halt a storm system.

Of course the dissipation time scale is a strong function of the spatial scale. Consider a cup of coffee. Say you add sugar to the coffee and stir it. How long do you have to wait for it to slow down? Assuming a cup 10 cm across, the dissipation time scale is:

$$T_\nu = \frac{L^2}{\nu} \approx \frac{(0.1\, m)^2}{10^{-5}\, m^2/sec} = 10^3\ sec$$

This is about 15 minutes. But coffee settles down much faster than this, perhaps over 15 seconds. We'll see why shortly.

Another important scaling can be obtained if we instead divide through the scales by fU, the size of the Coriolis term. Then we obtain:

$$\frac{\partial}{\partial t}u + \nabla \cdot (\vec{u}u) - f_z v = -\frac{1}{\rho_0}\frac{\partial}{\partial x}p + F^x + \nu\nabla^2 u$$

$$\frac{1}{fT} \qquad \frac{U}{fL} \qquad 1 \qquad \frac{P}{fU\rho_0 L} \qquad \frac{F}{fU} \qquad \frac{\nu}{fL^2} \tag{14}$$

The ratio of the advective term to the Coriolis term is thus U/fL. This is the *Rossby number*. This is also small at large scales. At *synoptic scales* (order 1000 km in the atmosphere), the Rossby number is roughly 0.1. Then the Coriolis term is 10 times larger than the advective term. Scaling the other terms, we find that the pressure gradient term is about the same size. So the dominant balance at weather scales is between the third and fourth terms, known as the *geostrophic balance*.

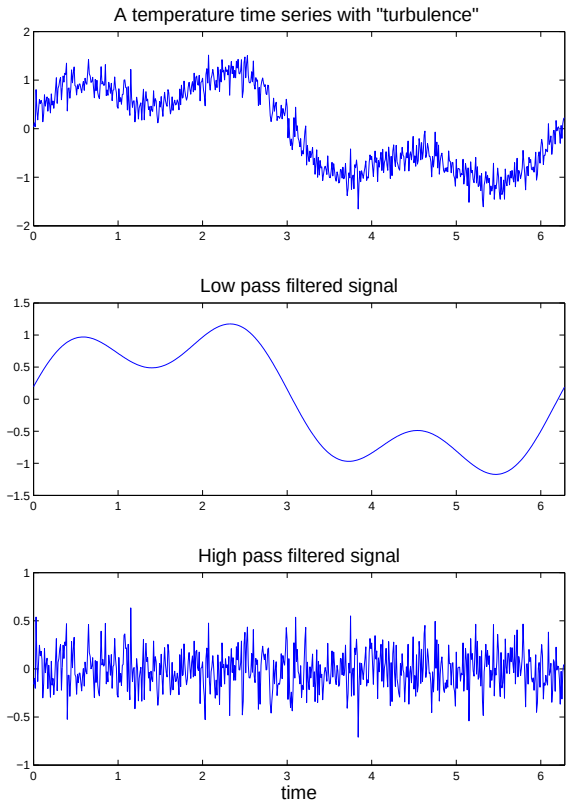

Figure 1: A time series of temperature measured over a certain period. The upper panel shows the whole time series, while the middle and lower panels show the low-pass and high-pass filtered time series.

2 Statistics in a nutshell

Turbulence often appears to be “noise” in a signal. Consider the temperature time series $T(t)$ in the upper panel of Fig. (1). The temperature varies slowly in time, but it also has a high frequency component. If we low-pass filter the time series, we get the signal in the middle panel. This has a smooth, even quasi-predictable looking, variation. If on the other hand we high-pass filter the time series, we get the signal in the lower panel. This appears to be “white noise”, i.e. a random signal with no dominant frequencies. This part of the signal looks completely unpredictable, i.e. we don’t know from one instant to the next how it will behave.

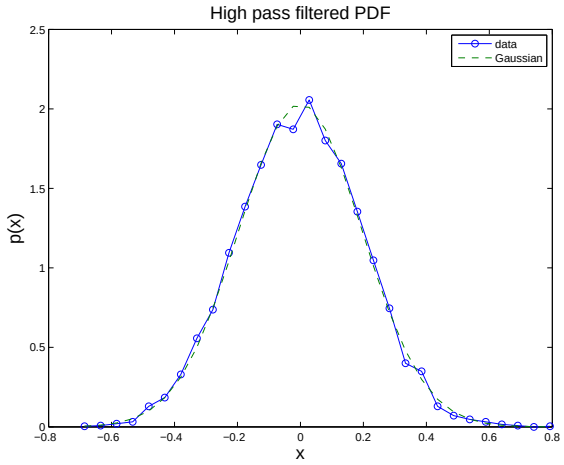

Figure 2: The probability density function (PDF) of the high-pass filtered time series in Fig. (1). The dashed curve is a Gaussian PDF.

Turbulence signals are often like in the lower panel. They are fundamentally unpredictable (we will demonstrate this in sec. 4). So rather than worrying about the exact values of the signal at any given time, we focus instead on *statistics*. We are more concerned about the range of possible values and the *moments*—the mean, the variance, etc.

The moments can be derived from the *probability density function* (PDF). To obtain this, we calculate a histogram from the signal by counting the number of times the temperature falls in selected ranges, e.g. between -0.2 and -0.1. Then we normalize the histogram so that:

$$\int_{-\infty}^{\infty} p(T)\, dT = 1 \tag{15}$$

The result shows us the probability of getting a particular value.

Fig. (2) shows the PDF for the high-pass filtered time series. We see that the value is most often around zero. But values as large as ± 0.7 occasionally occur.

The moments can be derived from the PDF. For example, the *mean*

temperature is:

$$< T >= \int_{-\infty}^{\infty} T p(T)\, dT \tag{16}$$

The mean for the distribution shown is -0.0022. This is close to zero, as we expected.

The width of the PDF is determined by the second moment, the *variance*:

$$V =< (T- < T >)^2 >= \int_{-\infty}^{\infty} (T- < T >)^2\, p(T)\, dT \tag{17}$$

For the distribution shown, the variance is 0.0386. A better indicator of the actual width though is the *standard deviation*, which is the root of the variance:

$$SD = (< (T- < T >)^2 >)^{1/2} \tag{18}$$

In the present case, this is 0.1965. You can see that the PDF falls to roughly half its maximum value at ± 0.2. This means that the temperature in the high pass filtered time series is most often between -0.2 and 0.2.

We can also calculate higher moments. The third order moment is the *skewness*:

$$S = \frac{\int_{-\infty}^{\infty} (T- < T >)^3\, p(T)\, dT}{SD^3} \tag{19}$$

It is traditional to normalize the skewness by the cube of the standard deviation so that the result is a non-dimensional number. The skewness indicates how asymmetric about the origin the distribution is. In our case, S=0.0271; the PDF is slightly skewed toward positive values.

The fourth order moment is also useful—this is the *kurtosis*:

$$K = \frac{\int_{-\infty}^{\infty}(T - < T >)^4 \, p(T) \, dT}{SD^4} \tag{20}$$

also occasionally called the "flatness" factor. The value reflects the shape of the PDF. If the PDF has a sharp peak in the middle and long wings, the kurtosis is large. In our case, k=2.9792.

If the kurtosis is near the value of three (as it is here), then the PDF is close to a *Gaussian* or "normal" distribution. The Gaussian is defined:

$$p(T) = \frac{1}{\sqrt{2\pi\delta^2}} \, exp(-\frac{(T - < T >)^2}{2\delta^2}) \tag{21}$$

This is indicated by the dashed curve in Fig. (2). We see our PDF is indeed close to normal.[1] It is advantageous having a Gaussian PDF because all the moments can be derived analytically.

3 The Fourier transform

Another operation we'll be using is the Fourier transform. The basic idea is that we project a function onto a basis of sinusoidal functions:

$$T(t) = \sum_{\omega} \hat{T}(\omega) e^{i\omega t} \tag{22}$$

where the sum goes over the range of the frequency, ω. We prefer the complex sinusoidal function because it's easier to work with than sines and cosines.

We can extract the component at a single frequency by Fourier transforming, thus:

[1] There is a theorem in statistics called the Central Limit Theorem which states that the sum of independent processes has a PDF which converges to a Gaussian.

$$\frac{1}{T}\int_0^T T(t)\, exp(-i\omega t)\, dt = \frac{1}{T}\int_0^T \hat{T}(\omega)\, dt = \hat{T}(\omega) \tag{23}$$

where T is, for example, the length of the record.

This is a Fourier transform in time. But the transform can be made in space as well. For instance, we can write:

$$\psi(x,y) = \sum_k \sum_l \hat{\psi}(k,l) e^{ikx+ily} \tag{24}$$

Then the corresponding transform is:

$$\hat{\psi}(k,l) = \frac{1}{L^2}\iint_0^L \psi(x,y) e^{-ikx-ily}\, dxdy \tag{25}$$

assuming that the domain extends from $[0, L]$.

An advantage of the Fourier transform is that it makes taking derivatives easy. If ψ above is the 2-D streamfunction, such that:

$$u = -\frac{\partial}{\partial y}\psi, \quad v = \frac{\partial}{\partial x}\psi \tag{26}$$

then:

$$\hat{u}(k,l) = -il\hat{\psi}(k,l), \quad \hat{v} = ik\hat{\psi} \tag{27}$$

Another useful point is concerns the energy. Say we have a domain with dimensions $x = [0, L]$ and $y = [0, M]$. The total kinetic energy in the domain is:

$$E = \frac{1}{LM}\iint \frac{1}{2}(u^2 + v^2)\, dxdy \tag{28}$$

The Fourier version of this is:

$$E = \frac{1}{2}\sum_k \sum_l \ |\hat{u}|^2 + |\hat{v}|^2 \tag{29}$$

Thus the kinetic energy is the sum of the squares of the Fourier amplitudes by wavenumber. This result is due to *Parseval's theorem*. Written in terms of the streamfunction, the energy is:

$$E = \frac{1}{2}\sum_k \sum_l (k^2 + l^2)|\hat{\psi}|^2 \tag{30}$$

Very often, we'll talk about the energy *spectrum*. This is just:

$$\mathcal{E}(k,l) = \frac{1}{2}(|\hat{u}|^2 + |\hat{v}|^2) \tag{31}$$

Then the total energy is the sum of the spectrum over all wavenumbers. The spectrum shows contribution to the energy by wavenumber (or frequency). This has traditionally been a central quantity in turbulence.

4 A chaotic example

As noted earlier, the "trouble" with the momentum equation is the quadratic nonlinearity on the LHS. It's useful to consider how this affects the solution in a simple case.[2] The x-momentum equation is again:

$$\frac{\partial}{\partial t}u + \nabla \cdot (\vec{u}u) - fv = -\frac{1}{\rho_0}\nabla p + F_x + \nu\nabla^2 u \tag{32}$$

We'll approximate this with a "toy" example:

$$\frac{d}{dt}u + ru^2 = 1 - u \tag{33}$$

[2]This example is based on one by Frisch (1995).

This has only a single variable, $u(t)$. The terms on the RHS are simple forcing and dissipation terms. The equation has a quadratic nonlinearity, and that is multiplied by r, which is essentially the Reynolds number for the problem. If r is small, the flow is viscous and the equation is approximately linear. If r is order one or larger, it is nonlinear.

We will discretize the equation, using a simple Euler routine with a time step $dt = 1$:

$$\frac{u(t+1) - u(t)}{1} + ru(t)^2 = 1 - u(t) \tag{34}$$

We can rewrite this as:

$$u(t+1) = F(u(t)) = 1 - ru(t)^2 \tag{35}$$

This is a variant of the "logistic map".[3]

The behavior of the system depends strongly on the parameter, r. If r is very small (less than 0.01), the solution approaches u=1.0. This is the viscous limit when the forcing determines the solution.

If r is larger than that, the solution approaches a smaller value. This is known as a *fixed point*. We find the fixed points by solving:

$$\frac{d}{dt}u = -ru^2 + 1 - u = 0 \tag{36}$$

This quadratic equation has solutions:

$$u = -\frac{1}{2r} \pm \frac{\sqrt{1+4r}}{2r} \tag{37}$$

There are two roots, one positive and one negative. With $r = 0.1$, the roots are $u = 0.9161$ and $u = -10.9161$. Solving (35) numerically (in Matlab),

[3]The logistic map was originally proposed in a paper by May (1976). His was an idealized model of a biological system where the growth rate of a population is proportional to the population itself. The paper became a landmark in the chaos literature.

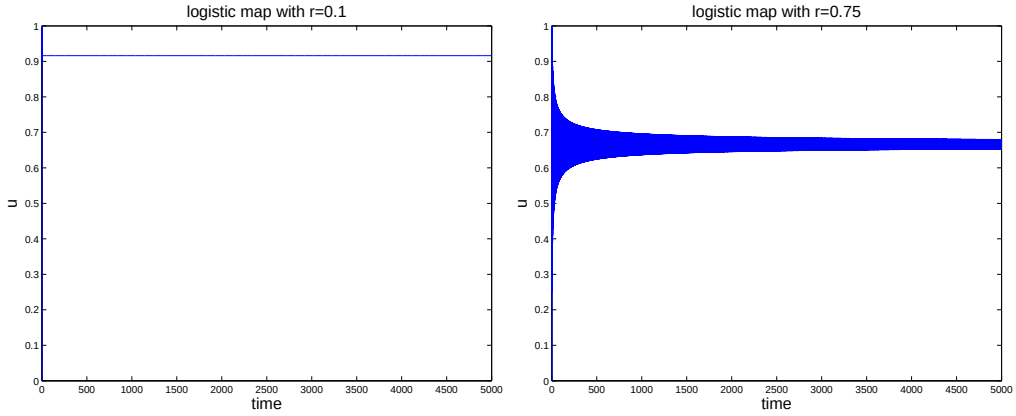

Figure 3: . Two solutions of the logistic map with u(0)=0. The solution at right has r=0.1 and the one on the right has r=0.75.

we see that the solution rapidly converges to the positive root (left panel of Fig. 3).

Why does it favor the positive root over the negative one? To see, we perform *linear stability analysis*. Let's say the solution is near a fixed point, denoted u_a. The fixed point is such that:

$$F(u_a) = u_a \tag{38}$$

So if we start at the fixed point, the mapping stays there. If we are near the fixed point, we can write:

$$u = F(u_a) + \delta(t) \tag{39}$$

where δ is a small deviation. Putting this into (35), we have:

$$u(t+1) = F(u_a) + \delta(t+1) = F(u_a + \delta(t)) \approx F(u_a) + F'(u_a)\delta(t) \tag{40}$$

after using a Taylor expansion. We keep only the first term, consistent with a "linear" analysis. Cancelling the $F(u_a)$ on both sides, we get:

$$\delta(t+1) = F'(u_a)\delta(t) \tag{41}$$

Whether $|\delta_t|$ increases or decreases depends therefore on $F'(u_a)$. If we think in terms of iterations, we have that:

$$\delta_{n+1} = (F'(u_a))\delta_n = (F'(u_a))^2\delta_{n-1} = (F'(u_a))^n\delta_1 \tag{42}$$

Thus if:

$$|F'(u_a)| < 1 \tag{43}$$

then δ will asymptote to zero. Note that if $0 < F'(u_a) < 1$, then δ decays monotonically to zero, while if $-1 < F'(u_a) < 0$, then δ oscillates as it decays. Likewise, if $F'(u_a) > 1$, δ increases monotonically and if $F'(u_a) < -1$, δ oscillates and increases. If δ decreases in time, then we say that u_a is a *stable* fixed point; if δ increases, it is an unstable fixed point.

We have that:

$$F'(u) = -2ru \tag{44}$$

With the positive root, $u_a = .9161$ so that $F'(u_a) = -0.1832$. So we expect decaying oscillations. In fact, there are oscillations in Fig. (3), but the decay is so rapid we don't see them. The other root, $u_a = 10.9161$ has $F'(u_a) = -2.1832$. Thus this point is unstable. So the numerical solution converges to the positive root rather than the negative one.

The oscillations are more noticeable when r is larger. An example, with $r = 0.75$, is shown in the right panel of Fig. (4). However, the solution is again approaching the positive root, which with $r = 0.75$ is $u = 2/3$. Note

that $F'(u_a) = -1$ in this case—so the linear stability analysis indicates we are on the border between stable and unstable solutions.

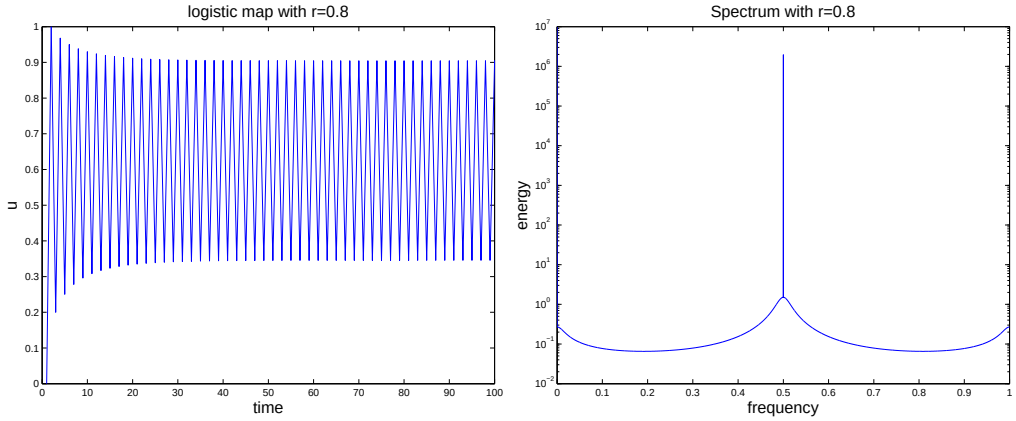

Figure 4: . The solution (left) and spectrum (right) with r=0.8.

Indeed, increasing r somewhat more, we find the oscillations don't die out. Consider the case with $r = 0.8$ (left panel of Fig. 4). Now u oscillates around the fixed point at $u = 0.6559$. An alternate way of looking at this is with the spectrum of u, as a function of the (non-dimensional) frequency, ω. There is a single peak at $\omega = 0.5$.

Increasing r further, the behavior becomes more complex. The case with $r = 1.3$ is shown in Fig. (5). We see that u is oscillating about the fixed point (at $u = 0.5731$), but the oscillations are less regular. Looking at the spectrum, we see why: there are now *three* dominant frequencies; the solution is a superposition of three waves.

Increasing r further, the solution becomes even more complex as more and more frequencies appear. With $r = 2$ (Fig. 6), the solution is fully *chaotic*; u oscillates between -1 and +1, but the motion is erratic and unpredictable. Sometimes there are rapid changes and sometimes slower ones. In addition, the spectrum (right panel) is nearly "white" (flat), indicating equal contributions across the range of frequencies.

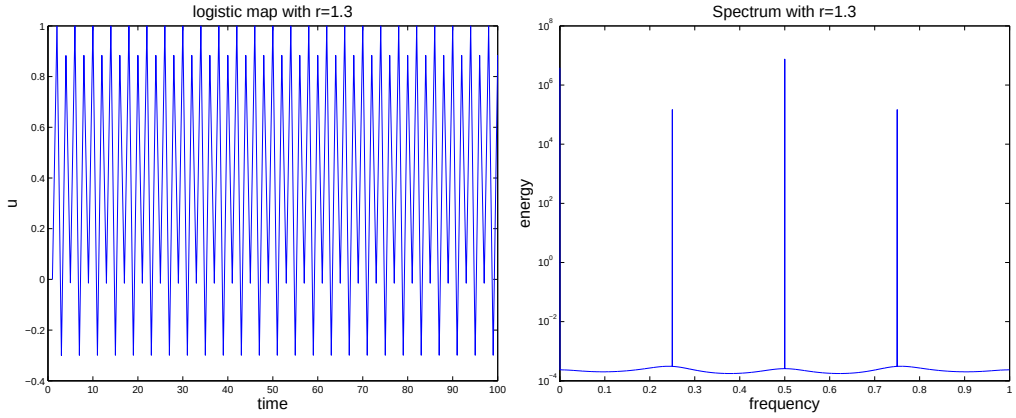

Figure 5: . The solution with r=1.3.

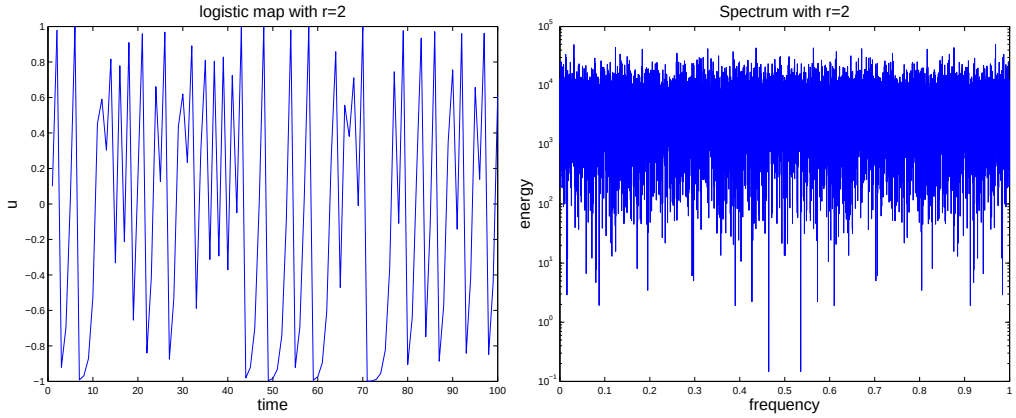

Figure 6: . The solution with r=2.

Chaos is implies that the system is sensitively dependent on the initial condition. The initial value in Fig. (6) is $u(0) = 0.1$. Let's change that slightly though to $u(0) = 0.10001$. The two curves are plotted in Fig. (7). We see that initially the curves are together. But shortly after t=10, they begin to diverge. And by t=20, the two are essentially independent of one another. This is a central difficulty with chaotic systems: unless you know the initial conditions *exactly*, it's impossible to make a correct prediction. And there will always be some error in the initial conditions.

Given that the motion is unpredictable, it doesn't make sense to worry

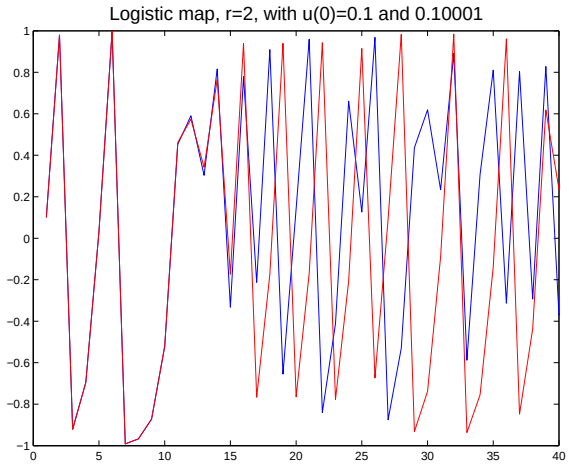

Figure 7: . The solution with r=2, with two initial values which are nearly the same.

about the exact value of u at any given time. Rather, we can focus on the statistics. The PDF of u is shown in Fig. (8) for both of the initial values used in Fig. (7). Despite that the two time series were very different, the PDFs are almost identical. We see that u takes on all values in the range from [-1:1]. We also see that u is most frequently near the extremes, -1 and 1. These are the extremes of the oscillations, so u spends more time in their neighborhood (the same is true for a simple sinusoidal oscillation). Note too that unlike with our noise example earlier, this PDF isn't remotely Gaussian. The kurtosis is roughly 1.5, well below the Gaussian value of 3.

With this value of r, it's actually possible to predict the shape of the PDF. Making a suitable change of variables (see Frisch, 1995), one can convert this to a "tent map", which has a *uniform* (or flat) PDF. Then one can convert back again to u to predict the PDF. The solution is:

$$p(u) = \frac{1}{\pi\sqrt{1-u^2}} \tag{45}$$

This is indicated by the red curve in Fig. (8).

There are several points here. One is that the system is fully chaotic at

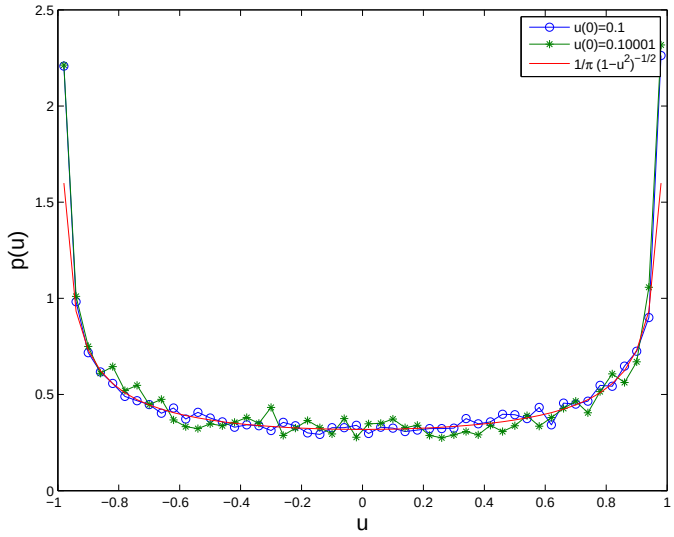

Figure 8: . The histogram of the logistic map with r=2 and 10,000 iterations. The red curve is the analytical prediction for this map, $p(u) = 1/(\pi\sqrt{1-u^2})$.

$r = 2$. If this is our Reynolds number, we see that the value is very low. With a Reynolds number of 10^{12}, as in the atmosphere, it isn't surprising the motion is chaotic.

Second, because u explores the entire range of values between -1 and 1, we say the motion is *ergodic*. Given (almost) any initial value, we can expect u to take on any other value in the range. Thus if we did an *ensemble* of experiments, measuring u at a point and then we averaged all the values we obtained, we would get the same answer if we just averaged u in time. We say that u is behaving in a probabilities way.

Lastly, we caution about taking the logistic map too literally. The progression from stable fixed points, to more and more oscillations to chaos is typical of nonlinear systems with few degrees of freedom. In the atmosphere or ocean, where there are many, many degrees of freedom, the transition from stability to chaos is usually less clean. Nevertheless, the logistic map gives us a good idea of what a quadratic nonlinearity can do.

Exercise: *Another map*

Analyze the equation:

$$\frac{du}{dt} + ru^2 = (r-1)u \tag{46}$$

with $dt = 1$.

a) Write the equation as a map.

b) What are the fixed points? Are they stable or not?

c) Write a Matlab code to solve the mapping. Check the solution for various values of r.

d) Write a second code to calculate the spectrum of u. Check the spectra in the cases in (b).

e) What are the critical values of r where transitions occur? When are the solutions fully chaotic? Plot time series to show this.

5 Conservation laws

Central in what follows are two *conservation laws*. These are for energy and enstrophy.

5.1 Energy

If we take the dot product of the momentum equation with the velocity, we get:

$$\frac{\partial}{\partial t}\frac{1}{2}|\vec{u}^2| + \nabla \cdot (\vec{u}\frac{1}{2}|\vec{u}^2|) = -\nabla \cdot [\vec{u}(\frac{p}{\rho_0} + gz)] + \vec{u} \cdot \mathcal{F} + \nu\vec{u} \cdot \nabla^2\vec{u} \tag{47}$$

We've used incompressibility to rewrite the pressure gradient/geopotential term. Note too that the Coriolis term has vanished—this is because it is perpendicular to the velocity.

We integrate this over a volume. We'll consider one of three types of (idealized) volume:

- A domain enclosed by solid walls
- A *periodic* domain, where flow out one side comes in the other side
- A channel (periodic in one direction, walled in the other)

At solid walls, the normal component of the velocity vanishes. With periodic conditions, the velocity is the same on opposite boundaries, so their difference is zero.[4]

The main effect is on the integral of divergences. Consider:

$$\iiint \nabla \cdot (\vec{u}G)\, dV = \oiint G\vec{u} \cdot \hat{n}\, dS = 0 \tag{48}$$

which is the advection of some quantity, G. By Gauss's theorem, the integral can be converted to a surface integral. This then vanishes with solid walls because the normal velocity is zero. With periodic boundary conditions, it also vanishes. Consider for example the integral in the x direction:

$$\int_0^L \frac{\partial}{\partial x}(uG)\, dx = u(L)G(L) - u(0)G(0) = 0 \tag{49}$$

By periodicity, the two terms are equal so their difference is zero.

Thus, if we integrate (47) over the volume, we get:

$$\frac{d}{dt}E = \iiint \vec{u} \cdot \mathcal{F}\, dV + \nu \iiint \vec{u} \cdot \nabla^2 \vec{u}\, dV \tag{50}$$

where:

[4]Boundaries can be important places, supporting boundary layers which are sometimes turbulent themselves. We purposely avoid such issues here.

$$E = \iiint \frac{1}{2}|\vec{u}^2|\, dV \tag{51}$$

is the total kinetic energy. This states that the total energy changes only in response to forcing and dissipation. Advection doesn't change the total energy; it only redistributes energy in the domain. Dissipation causes the energy to *decrease*. To see this, we use a vector identity:

$$\nabla^2\vec{u} = \nabla(\nabla\cdot\vec{u}) - \nabla\times(\nabla\times\vec{u}) = -\nabla\times\vec{\omega} \tag{52}$$

where $\vec{\omega}$ is the total vorticity. The first term vanishes by incompressibility. Taking the dot product with $\vec{u}$, we get:

$$\vec{u}\cdot\nabla^2\vec{u} = -\vec{u}\cdot(\nabla\times\omega) = -\vec{\omega}\cdot(\nabla\times\vec{u}) + \nabla\cdot(\vec{\omega}\times\vec{u}) \tag{53}$$

using another vector identity. Now when we integrate over space, the last term vanishes:

$$\iiint \nabla\cdot(\vec{\omega}\times\vec{u})\, dV = \oiint(\vec{\omega}\times\vec{u})\cdot\hat{n}\, dS = 0 \tag{54}$$

So we can write:

$$\nu\iiint \vec{u}\cdot\nabla^2\vec{u}\, dV = -\nu\iiint \vec{\omega}\cdot(\nabla\times\vec{u})\, dV = -\nu\iiint |\vec{\omega}|^2\, dV \tag{55}$$

So the energy equation, without forcing, is:

$$\frac{d}{dt}E = -\nu\iiint |\vec{\omega}|^2\, dV \tag{56}$$

The energy dissipation is proportional to the integral of the squared vorticity, also known as the *enstrophy*. Because the RHS is negative definite, the energy can only decrease in time.

A question which will become important later on is whether the energy is *conserved* when the viscosity goes to zero. It could happen that the enstrophy increases as ν decreases. Say for example that:

$$\iiint |\vec{\omega}|^2 \, dV \propto \frac{C}{\nu} \tag{57}$$

in the limit of small viscosity. Then we would have

$$\frac{dE}{dt} = -C \tag{58}$$

regardless of how small ν was. For this to happen, there must be *production* of vorticity in the absence of forcing (i.e. the vorticity doesn't just decrease). To see whether or not this is the case, we turn to the vorticity equation.

5.2 Vorticity and enstrophy

We get the vorticity equation by taking the curl of the momentum equation. This calculation is easier if we first rewrite the momentum equation thus:

$$\frac{\partial}{\partial t}\vec{u} + (\vec{\omega} + 2\vec{\Omega}) \times \vec{u} = -\nabla(\frac{p}{\rho_0} + \frac{1}{2}|\vec{u}^2| + \Phi_g) + \mathcal{F} + \nu\nabla^2\vec{u} \tag{59}$$

Taking the curl, we get:

$$\frac{\partial}{\partial t}\vec{\omega} + \vec{u} \cdot \nabla\vec{\omega}_a + \vec{\omega}_a(\nabla \cdot \vec{u}) = \vec{\omega}_a \cdot \nabla\vec{u} + \nabla \times \mathcal{F} + \nu\nabla^2\vec{\omega} \tag{60}$$

where:

$$\vec{\omega}_a = \nabla \times \vec{u} + 2\vec{\Omega}$$

is the *absolute vorticity*. The third term vanishes by incompressibility. Assuming for the moment that the rotation vector, $\vec{\Omega}$ is constant, we're left with:

$$\frac{d}{dt}\vec{\omega} = \vec{\omega}_a \cdot \nabla\vec{u} + \nabla \times \mathcal{F} + \nu\nabla^2\vec{\omega} \tag{61}$$

The question is whether the enstrophy, $|\vec{\omega}|^2$ will be bounded if there is no forcing ($\mathcal{F} = 0$) and if the viscosity, ν, is decreased toward zero. Multiplying by $\vec{\omega}$, we obtain:

$$\frac{1}{2}\frac{d}{dt}|\vec{\omega}|^2 = \vec{\omega} \cdot (\vec{\omega}_a \cdot \nabla\vec{u}) + \nu\vec{\omega} \cdot \nabla^2\vec{\omega} \tag{62}$$

Integrating this in space, and using the same vector identities that we did with the energy, we obtain:

$$\frac{d}{dt}\iiint \frac{1}{2}|\vec{\omega}|^2 \, dV = \iiint \vec{\omega} \cdot (\vec{\omega}_a \cdot \nabla\vec{u}) \, dV - \nu \iiint |\nabla \times \vec{\omega}|^2 \, dV \tag{63}$$

The last term is negative definite, causing a decay in the enstrophy. But the middle term has an undetermined sign—in fact, this can act as a source of enstrophy. So we cannot say whether E is conserved in the limit of vanishing viscosity. What happens in such high Reynolds number fluids is that the velocity gradients become very large at small scales. So the enstrophy can be very large.

However, this isn't the case in *two* dimensions. In this case, the velocity is purely horizontal:

$$\vec{u} = (u, v, 0) \tag{64}$$

The vorticity, which is perpendicular to the velocity, is purely *vertical*:

$$\vec{\omega} = (0, 0, \frac{\partial}{\partial x}v - \frac{\partial}{\partial y}u) \equiv \zeta\hat{k} \tag{65}$$

In addition, the planetary rotation vector is predominantly vertical at large scales:

$$2\vec{\Omega} \approx 2\Omega sin(\theta)\hat{k} \equiv f\hat{k} \tag{66}$$

So:

$$\omega_a \cdot \nabla\vec{u} = (\zeta + f)\hat{k} \cdot \nabla(u\hat{i} + v\hat{j}) = 0 \tag{67}$$

So the source of enstrophy is absent in a 2-D flow and that the enstrophy can only decrease in time. This means the energy *is* conserved in the inviscid limit in 2-D, i.e.

$$lim_{\nu \to 0} \frac{dE}{dt} = 0 \tag{68}$$

This has an enormous effect on 2-D flows.

But is the enstrophy conserved in 2-D with vanishing viscosity? Without the production term, the RHS of equation (63) is negative definite. But it is not guaranteed that enstrophy is conserved unless we know that curl of the vorticity is bounded in this limit. To see that, we have to consider the next equation, for the *palinstrophy*. It turns out there is a source term for that as well. So we can't assume enstrophy is conserved—just as we couldn't assume energy was conserved in 3-D.

Thus in the limit $\nu \to 0$, the energy is conserved in 2-D. In 3-D, it isn't necessarily conserved. What we will see is that even if ν is minuscule, the energy can decrease in 3-D. But this doesn't happen in 2-D. This suggests

that energy isn't affected by the dissipation at very small scales in 2-D. We'll see why shortly.

6 3-D turbulence

Now we return to the coffee cup. Why does it spin down so quickly? More specifically, how can dissipation, acting at molecular scales, affect the energy at the scale of the coffee cup? We'll see that this has to do with how energy is exchanged between scales. To understand that better, we turn first to the energy.

6.1 Triad interactions

To understand how energy is transferred between scales, we will work in Fourier space. Imagine the forcing, $\mathcal{F}$, happens at large scales. This is the spoon stirring the coffee. Assume too the dissipation is at the molecular scale. This implies that there is a range of *intermediate* scales where the forcing and dissipation aren't relevant. At these scales, it is advection which dominates the changes in the velocity.

We can illustrate how this works by focusing on just one of the advective terms, in the x-momentum equation:

$$\frac{\partial}{\partial t}u = -u\frac{\partial}{\partial x}u \tag{69}$$

We first write the velocity on the LHS in terms of its Fourier transform:

$$u = \sum_k \hat{u}(\vec{k}, t)\, e^{ik_x x + ik_y y + ik_z z} \tag{70}$$

The summation is over the three wavenumbers, (k_x, k_y, k_z). The RHS involves the product of two velocities. As such, we need two different trans-

forms:

$$-u\frac{\partial}{\partial x}u = -\sum_l \sum_m m_x \hat{u}(\vec{l},t)\,\hat{u}(\vec{m},t)\,e^{i(l_x+m_x)x+i(l_y+m_y)y+i(l_z+m_z)z} \quad (71)$$

The factor of m_x comes from taking the x-derivative.

Now let's take the Fourier transform of the LHS. We multiply both sides the whole equation by $exp(-ik_x x - ik_y y - ik_z z)$ and integrate over the domain. On the RHS, we have an integral like:

$$\frac{1}{L^3}\iiint_0^L e^{i(l_x+m_x-k_x)x+i(l_y+m_y-k_y)y+i(l_z+m_z-k_z)z}$$

If:

$$\vec{k} = \vec{l} + \vec{m}$$

Then the integral is one. If not, the integral is zero.[5] Thus the result is:

$$\frac{\partial}{\partial t}\hat{u}(\hat{k},t) = -\sum_l \sum_m m_x\,\hat{u}(\vec{l},t)\,\hat{u}(\vec{m},t)\,\delta(\vec{l}+\vec{m}-\vec{k}) \quad (72)$$

where:

$$\delta(x) = \begin{cases} 1 & \text{if } x = 0 \\ 0 & \text{if } x \neq 0 \end{cases}$$

is the delta function. The same result would obtain if we had simply applied the *convolution theorem*. The results shows that wave interactions occur between groups of three waves, or *triads*.[6]

So a wave with $\vec{k} = (3,3,0)$ will interact with waves with $(1,2,0)$ and $(2,1,0)$. This is known as a *local* interaction, because the wavenumbers for the triad are all similar. But the same wave will also be affected by the

[5] Actually, we assume we have an integral number of wavenumbers in the domain. So for example $k_x = n\pi/L$.

[6] The triad interaction can also be derived directly from the convolution theorem of Fourier transforms.

waves with $(-10, 2, 0)$ and $(13, 1, 0)$. These have a much smaller scale in the x-direction. This is a *non-local* interaction, as the components have very different sizes.

Consider Fig. (9), which shows a hypothetical energy spectrum, $\mathcal{E}$. We plot the spectrum as a function of the total wavenumber:

$$\kappa \equiv (k_x^2 + k_y^2 + k_z^2)^{1/2}$$

The wavenumber is on the x-axis. Note that increasing wavenumber implies *decreasing* size; so the large scales are on the left. Now the fluid is forced at a large scale, perhaps by the spoon in the cup. This produces an energy spectrum like that in dash-dot line—a spike at the forcing scale. Interactions between wavenumbers cause the spectrum to spread out, as the energy is transferred to other wavenumbers. Local interactions cause the energy to *cascade* to smaller scales (larger wavenumbers). At later times, there is energy across a range of wavenumbers. Then non-local interactions can occur, between large and small scale waves.

Eventually energy arrives at the smallest scales, where it is dissipated by molecular interactions. So this is how molecular dissipation can bring the coffee to rest: because turbulence transfers energy down to the dissipation scales.

Exercise: *2-D triads*

Triad interactions also occur in 2-D. In this case, we can write the vorticity equation as:

$$\frac{\partial}{\partial t}\zeta + u\frac{\partial}{\partial x}\zeta + v\frac{\partial}{\partial y}\zeta = 0 \tag{73}$$

In 2-D, the velocity and vorticity can be written in terms of a streamfunc-

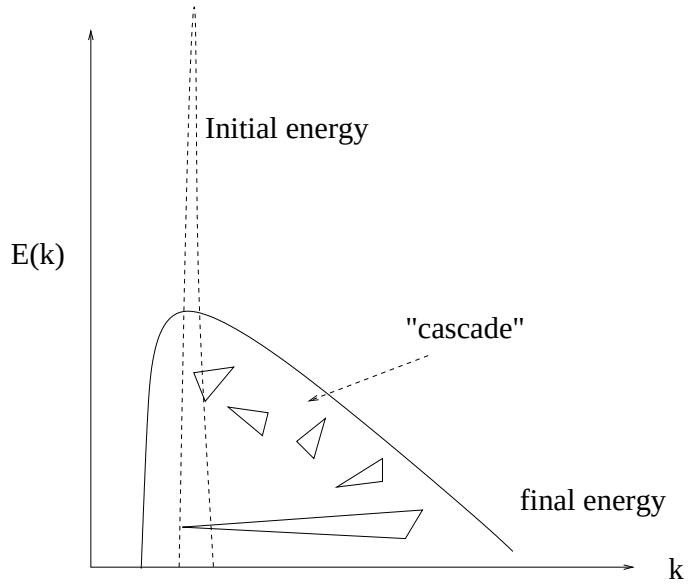

Figure 9: A hypothetical cascade of an initially narrow band energy spectrum to smaller scales. We imagine that energy is conserved during the cascade, so that the area under the curves is conserved (despite appearances).

tion:

$$u = -\frac{\partial}{\partial y}\psi, \quad v = \frac{\partial}{\partial x}\psi, \quad \zeta = \frac{\partial}{\partial x}v - \frac{\partial}{\partial y}u = \nabla^2\psi \tag{74}$$

Say that:

$$\psi = \sum_k \sum_l \hat{\psi}(k,l) e^{ik_x x + ik_y y} \tag{75}$$

Fourier transform the vorticity equation, assuming a domain with lengths 2π in each direction. Substitute in the expansions above and obtain an equation for $\frac{\partial}{\partial t}\psi(\vec{k})$. Show that the advective terms contribute in triads.

6.2 Kolmogorov's inertial range

Thus forcing puts energy into the system and dissipation removes it. We assume the forcing happens at much larger scales than the dissipation, which happens on molecular scales, and that there is a range of scales in between

where neither forcing or dissipation are important. As the great British scientist, Lewis Fry Richardson put it:

Big whirls have little whirls,
that feed on their velocity.
And little whirls have littler whirls,
and so on to viscosity.

Kolmogorov proposed a theory in 1941 for this transfer, which has become known as the *inertial range*. The theory employs a number of assumptions:

- We assume the turbulence is *isotropic*—the same in all directions. So instead of using $E(k, l, m)$, we can focus on $E(\kappa)$, where κ is the magnitude of the wavenumber vector.
- We also assume the turbulence is *homogeneous*—the same at all locations in space. So we can speak about the dynamics in wavenumber space, without worrying about variations from place to place.
- And we assume that triad interactions are *local*. This reason for this will become clearer later on.

As stated, the details of the forcing and dissipation don't matter in the inertial range. Thus the *only* important parameter in the inertial range is the rate at which energy is transferred downscale. We call this the energy flux, ϵ.

Now the spectrum, $E(k)$, has dimensions of L^3/T^2. That's because energy has units of L^2/T^2, and the energy is the sum over wavenumbers of the spectrum (and the wavenumber has units of L^{-1}). The flux on the

other hand has units of L^2/T^3, proportional to energy over time. So from dimensional considerations alone, we can see that:

$$E(k) = C\epsilon^{2/3}k^{-5/3} \tag{76}$$

where C is a constant.

The inertial range begins near the forcing scale. It extends down to a scale where dissipation begins to be important. We can deduce this scale by equating time scales. The dissipation time scale, mentioned before, is:

$$T_\nu \propto \frac{L^2}{\nu} \propto \nu^{-1}k^{-2} \tag{77}$$

The cascade time scale can be deduced from the flux from dimensions:

$$T_a \propto \epsilon^{-1/3}k^{-2/3} \tag{78}$$

In the dissipation range, the dissipation time scale is shorter than the cascade time scale, because energy decays before it is transferred. The opposite is true in the cascade range. At the transition between the cascade and the dissipation ranges, the two scales are equal. Equating them, we get:

$$k_\nu = (\frac{\epsilon}{\nu^3})^{1/4} \tag{79}$$

The corresponding length scale, $L_\nu = (\nu^3/\epsilon)^{1/4}$, is now called the *Kolmogorov scale*. This marks the boundary between the inertial and dissipative ranges.

The Kolmogorov formulation is also self-consistent with regards to dissipation. As noted earlier, the energy dissipation rate is given by:

$$D = -\nu \iiint |\vec{\omega}|^2 \, dV$$

The term in the integral has a scale:

$$\frac{\nu U^2}{L^2} \propto \nu k^2 U^2$$

U^2 scales as the total energy, or $\epsilon^{2/3} k^{-2/3}$. So the energy dissipation (per unit volume) scales as:

$$D \propto \nu \epsilon^{2/3} k^{4/3}$$

At the dissipation wavenumber, k_ν, this equals

$$\nu\, \epsilon^{2/3}\, \frac{\epsilon^{1/3}}{\nu} = \epsilon$$

So the dissipation rate is equal to the energy flux across the inertial range. The Kolmogorov construct is self-consistent in that the amount of energy put in by the forcing is removed by dissipation.

But notice something—the dissipation rate is *independent of* ν! Imagine that we make ν smaller and smaller. Then the dissipation scale L_ν is similarly smaller. But the dissipation *rate* is the same. The only difference is that the inertial range carries the energy to smaller scales.

This is a critical point. Because of the downscale cascade, energy will not be conserved in a 3-D fluid, so long as there is even an infinitesimal amount of dissipation. Energy can only be conserved if there is identically *zero* dissipation, which can never be realized.

The Kolmogorov picture can be illustrated as in Fig. (10). The energy is injected at wavenumber, κ_f, and at a rate ϵ. It then cascades downscale at the same rate, ϵ, to the dissipation wavenumber, κ_ν, where it is dissipated at the same rate. In the inertial range, the only parameter which matters is ϵ, yielding the characteristic $\kappa^{-5/3}$ spectrum.

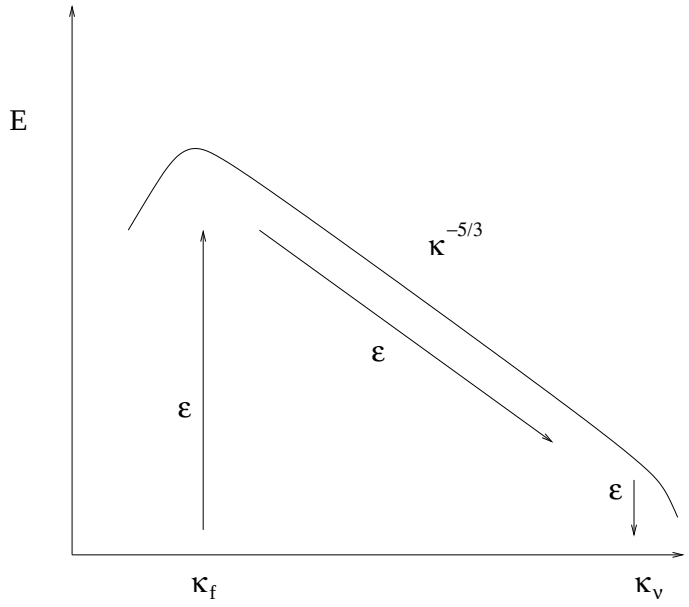

Figure 10: The Kolmogorov energy spectrum.

6.3 Shell models

A simple way to understand the Kolmogorov model is as follows. Imagine the turbulence involves energy transfer between discrete wavenumber bins (Fig. 11). In the figure, we have four bins, and so four different scales of wave. Energy enters at the largest scale ($k = 1$) and is removed by dissipation at the smallest scale ($k = 8$).

In drawing the figure this way, we make the assumption that the wavenumber interactions are *local*. Thus energy transfer occurs only between adjacent bins. The situation would be much more complicated if we allowed for transfer between all the bins.

The rate that energy is transferred from $k = 1$ to $k = 2$ is given by ϵ. This is the same rate as energy is transferred to $k = 4$. Imagine this were not so. Say the energy transfer from $k = 2$ to $k = 4$ was only $\epsilon/2$. Then the energy would be entering the $k = 2$ bin faster than it was leaving, and

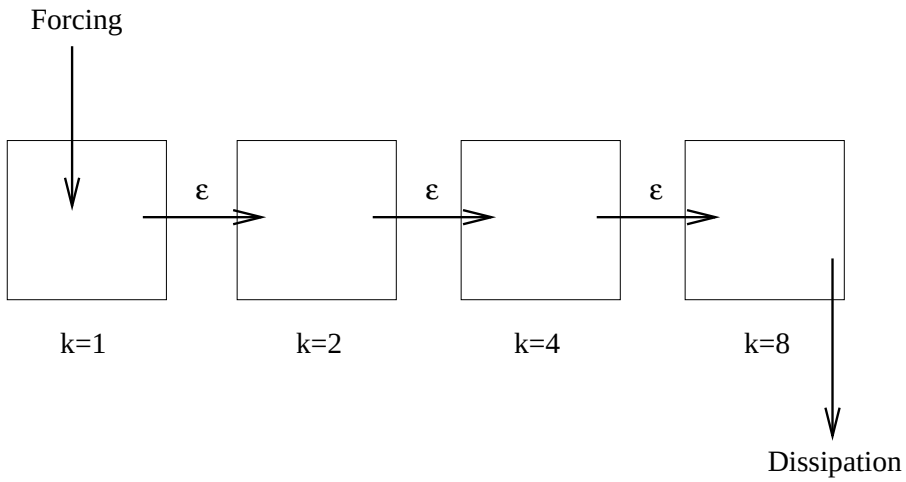

Figure 11: Energy transfer in the shell model. Energy is put in at the largest scale ($k = 1$) and removed at the smallest ($k = 8$).

the energy in the bin would increase in time. The spectrum then would not be stationary in time. So the transfer rate must be the same between all bins.

Also notice that the rate that energy is removed from the last bin ($k = 8$) is also ϵ. So the dissipation rate is equal to the flux. Again, if this weren't so, the energy would pile up in the smallest bin.

In fact, this is a real possibility. In numerical models with too little dissipation, the energy cascades to the smallest scales faster than it's taken out. So the energy increases at the smallest scales and the model subsequently blows up. The shell model illustrates why this is so.

Exercise: *Structure functions*

Kolmogorov (1941) did not actually derive the form of the energy spectrum. Rather, he derived relations for the velocity *structure functions*. These are powers of the velocity difference between two points. For example, the second order structure function is:

$$S(r) =< |u(\vec{x}+r) - u(\vec{x})|^2 > \tag{80}$$

The brackets indicate an *ensemble* average, i.e. an average over a number of observations. Use dimensional analysis to deduce how $S(r)$ varies with the separation, r. Compare this to the spectrum. Consider also the third order structure function, which has a special significance in turbulence theory.

6.4 Observations

Observations support Kolmogorov's prediction for the energy spectrum. An example is shown in Fig. (12), from measurements in a jet in the laboratory (Champagne, 1978). The $k^{-5/3}$ dependence is seen clearly over roughly two decades of wavenumber.

Another well-known example is the observations of Grant et al. (1962) in a tidally-mixed fjord on the west coast of the US. This also yielded strong evidence of a $k^{-5/3}$ spectrum (Fig. 13).

There are numerous other examples as well, from the atmospheric boundary layer, in laboratory experiments and in numerical simulations.

However, where the model is less successful is at predicting the *higher moments*. Energy, like the variance, is a second order statistic, being proportional to the velocity squared. But one can also look at higher powers, such as the skewness and the kurtosis. Or, one can look at velocity PDFs.

What is typically found is that the differences between velocities at separated points (see the exercise above on structure functions) are not Gaussian. As shown in Fig. (14), the PDFs for velocity differences with large separations are close to Gaussian. But as the separation, r, approaches the

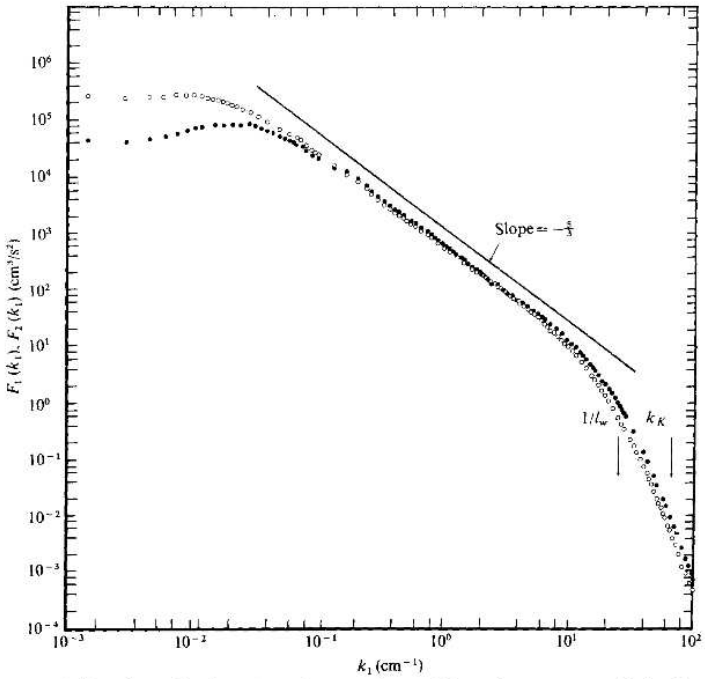

FIGURE 15. One-dimensional spectra of streamwise- and lateral-component velocity fluctuations for an axisymmetric jet; $Re = 3{\cdot}7 \times 10^6$, $x/d = 70$, $r/d = 0$. ○, $F_1(k_1)$; ●, $F_2(k_1)$.

Figure 12: The energy spectra for the stream-wise and transverse velocity components in a jet, with $Re = 626$. From Champagne (1978).

Kolmogorov scale, the wings of the PDFs become more and more extended.

What this implies is that while the velocities themselves may have an approximately Gaussian distribution, the velocity *gradients* are not Gaussian. What one sees if one measures the gradients is that large values occasionally occur, much larger than would be expected for a Gaussian process. Such episodes appear as "bursts" in the time series. We say that the turbulence is "intermittent".

This can be taken into account in the shell model above, by stating that the turbulence fills only a fraction of the bins. This is the idea behind the "β-model". Such a model yields the same spectra as Kolmogorov, but predicts deviations in the higher moments, as observed.

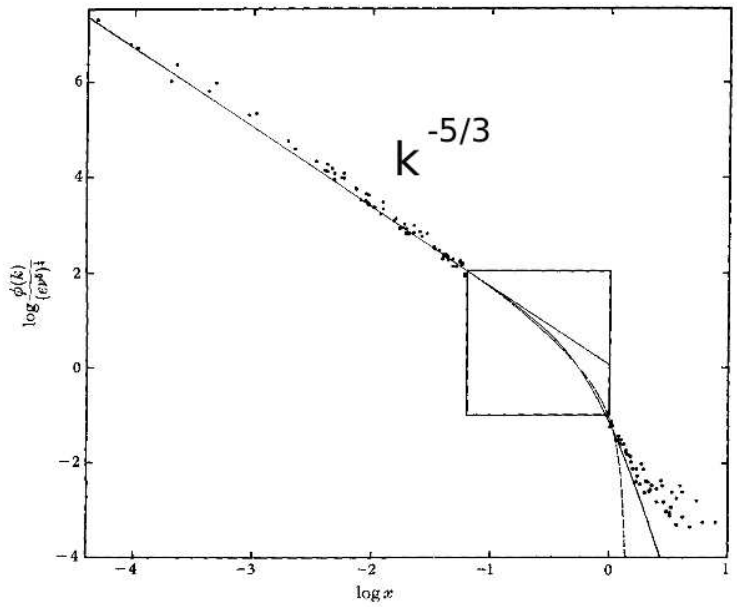

FIGURE 12. Seventeen spectra compared to the theories of Kolmogoroff, Heisenberg and Kovasznay. The straight line has a slope of $-\frac{5}{3}$, the curved solid line is Heisenberg's theory and the dashed line is Kovasznay's theory. Within the square, the observations are too crowded to display on this scale and they are shown in figure 13.

Figure 13: Energy spectrum from towed measurements in a tidal basin by Grant et al. (1962). The boxed region shows the region of transition to the dissipative range.

7 2-D turbulence

At synoptic scales in the atmosphere and ocean, the motion is more nearly two dimensional than three dimensional. This is because the vertical velocity, suppressed by rotation, is much smaller than the horizontal velocities. Turbulence in two dimensions is similar to that in 3-D, but also quite different.

We take the motion to be identically two-dimensional, so that the velocity is given by:

$$\vec{u} = (u, v, 0) \tag{81}$$

Now the continuity equation is just:

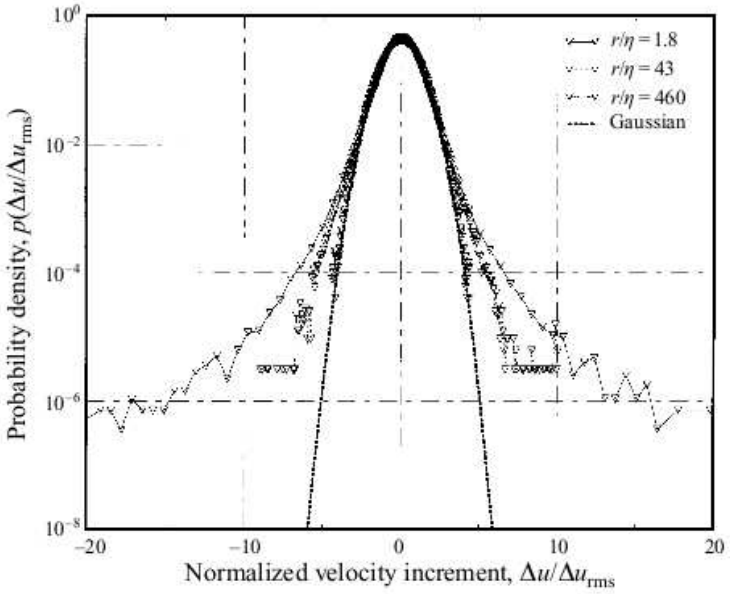

Figure 14: PDFs of the velocity differences for different separations, r. At the largest separations, near the forcing scale, the PDFs are nearly Gaussian. But approaching the Kolmogorov scale, the wings of the PDF become more and more extended.

$$\frac{\partial}{\partial x}u + \frac{\partial}{\partial y}v = 0 \tag{82}$$

This implies we can write the velocities in terms of a streamfunction, ψ:

$$u = -\frac{\partial}{\partial y}\psi, \quad v = \frac{\partial}{\partial x}\psi \tag{83}$$

The vorticity is perpendicular to the velocity, so it only has a vertical component:

$$\vec{\omega} = (\frac{\partial}{\partial x}v - \frac{\partial}{\partial y}u)\,\hat{k} = \nabla^2\psi \tag{84}$$

We usually refer to the 2-D vorticity as ζ. The equation for the 2-D vorticity follows from (61):

$$\frac{\partial}{\partial t}\zeta + \vec{u}\cdot\nabla(\zeta + f) = \nabla\times\mathcal{F} + \nu\nabla^2\zeta \tag{85}$$

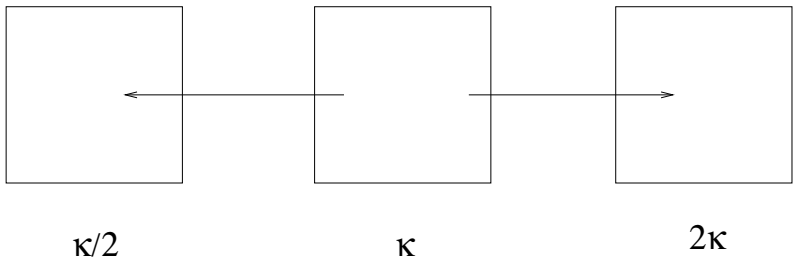

Figure 15: A triad in two dimensions. Energy flows from the center box to the other two. Each box has a scale which is twice that of the box to it's right.

As noted earlier, the vorticity production term is absent because the vorticity and velocity are perpendicular.

7.1 A triad interaction

The interesting aspect about 2-D turbulence is illustrated nicely in an article by Fjørtoft (1953).[7] We look at a triad interaction between three wavenumbers, as illustrated in Fig. (15). Energy is initially in the center box, at wavenumber k. The energy flows to the other two boxes, one which has waves twice as large $\kappa/2$ and the other twice as small 2κ. The energy in the boxes is E_0, E_1 and E_2, going from left to right.

Fjørtoft takes $\nu = 0$, so that both the energy and enstrophy are conserved. This is a reasonable assumption in the inertial range, where dissipation is unimportant. Thus:

$$E_0 + E_2 = E_1 \tag{86}$$

and:

$$Z_0 + Z_2 = Z_1 \tag{87}$$

[7] A remarkable, short paper...with no references! Fjørtoft argues all his points on first principles.

Now these two statements are related to each other, as follows.

The energy in 2-D is:

$$E = \frac{1}{2}(u^2 + v^2) = \frac{1}{2}(k^2 + l^2)\psi^2 \tag{88}$$

The enstrophy on the other hand is:

$$Z = \frac{1}{2}(\frac{\partial}{\partial x}v - \frac{\partial}{\partial y}u)^2 = \frac{1}{2}(k^2 + l^2)^2\psi^2 = \kappa^2 E \tag{89}$$

So the enstrophy conservation statement for the boxes can be written:

$$\kappa_0^2 E_0 + \kappa_2^2 E_2 = \kappa_1^2 E_1 \tag{90}$$

Using our values for the wavenumbers, we have:

$$\frac{\kappa^2}{4}E_0 + 4\kappa^2 E_2 = \kappa^2 E_1 \tag{91}$$

or simply:

$$\frac{1}{4}E_0 + 4E_2 = E_1 \tag{92}$$

We can combine this with the energy equation to obtain:

$$E_0 = \frac{4}{5}E_1, \quad E_2 = \frac{1}{5}E_1 \tag{93}$$

Thus 80% of the energy goes to the *larger* scale wave. Energy is apparently going upscale rather than downscale!

What about the enstrophy? We have:

$$Z_0 = \frac{\kappa^2}{4}E_0 = \frac{\kappa^2}{4}\frac{4}{5}E_1 = \frac{1}{5}Z_1 \tag{94}$$

Similarly, we find:

$$Z_2 = \frac{4}{5} Z_1 \tag{95}$$

So the situation is reversed: 80% of the enstrophy goes to the smaller wave.

If you use different size waves, you will find different fractions of energy and enstrophy transfer. But as shown by Merillees and Warn (1975), most triads nevertheless act as the one above and transfer energy to larger scales.

Exercise: *Another triad*

Consider the general case where $\kappa_0 = \kappa_1/n$ and $\kappa_2 = n\kappa_1$. What fraction of energy goes to the larger wavenumber and what fraction to the smaller. What about the enstrophy?

7.2 An integral argument

Another way to see this was proposed by Batchelor (1953), pretty much on the last page of his seminal book *Homogeneous Turbulence*. Imagine we have a narrow energy spectrum initially, as in Fig. (9). The spectral peak will broaden in time, as energy is passed to other wavenumbers via triad interactions. We can express this as:

$$\frac{d}{dt} \int (\kappa - \kappa_i)^2 \, E \, d\kappa > 0 \tag{96}$$

where κ_i is the wavenumber peak of the initial spectrum. Expanding the LHS, we get:

$$\frac{d}{dt} [\int \kappa^2 \, E \, d\kappa - 2\kappa_i \int \kappa \, E \, d\kappa + \kappa_i^2 \int E \, d\kappa] > 0 \tag{97}$$

Now the first term is the enstrophy and the last term is proportional to the total energy, both of which are constant in time. So we must have:

$$\frac{d}{dt}\int \kappa\, E\, d\kappa < 0 \tag{98}$$

Written another way, this is:

$$\frac{d}{dt}\left(\frac{\int \kappa\, E\, d\kappa}{\int\ E\, d\kappa}\right) = \frac{d}{dt}\kappa_m < 0 \tag{99}$$

Thus κ_m, the mean wavenumber of the spectrum, is *decreasing in time*. That implies that the spectrum is shifting to the left, toward larger scales. Consistent with Fjørtoft, Batchelor concludes that energy is moving up-scale in 2-D.

We can use a similar argument to see what's happening to the enstrophy (Salmon, 1998). If the spectrum is spreading, we also can write:

$$\frac{d}{dt}\int (\kappa^2 - \kappa_i^2)^2\, E\, d\kappa > 0 \tag{100}$$

Expanding this, we get:

$$\frac{d}{dt}\left[\int \kappa^4\, E\, d\kappa - 2\kappa_i^2 \int \kappa^2\, E\, d\kappa + \kappa_i^4 \int E\, d\kappa\right] > 0 \tag{101}$$

The second term is proportional to the total enstrophy, and the last term to the total energy. So we have:

$$\frac{d}{dt}\int \kappa^4\, E\, d\kappa = \frac{d}{dt}\int \kappa^2\, Z\, d\kappa > 0 \tag{102}$$

So:

$$\frac{d}{dt}\frac{\int \kappa^2\, Z\, d\kappa}{\int\ Z\, d\kappa} > 0 \tag{103}$$

Thus the mean square wavenumber for the enstrophy is *increasing* in time; the enstrophy spectrum is shifting to the right, toward small scales.

Thus *two* cascades are occurring simultaneously in 2-D: there is an energy cascade to larger scales, and an enstrophy cascade to smaller scales. That implies that there are two cascade ranges.

Exercise: *Batchelor, part 2*

Re-do Batchelor's arguments using the *mean* wavenumber instead of the initial wavenumber. Assume that the variance in wavenumber increases in time. Do you get the same results?

7.3 The two inertial ranges

That there are two inertial ranges in forced 2-D turbulence was realized by Kraichnan (1967), Leith (1968) and Batchelor (1969). We assume the fluid is forced and that the spectrum is stationary (not changing in time), just as in the Kolmogorov case in 3-D.

As noted, there are two inertial ranges. One is the energy cascades range. Dimensionally, this is exactly the same as in the Kolmogorov case. The energy cascades at a rate ϵ, and the spectrum has the form:

$$E(\kappa) = C\epsilon^{2/3}\kappa^{-5/3} \tag{104}$$

exactly as in three dimensions. The only difference is the direction of transfer, which is now *upscale*. So if the forcing were, say, at the 1 km scale, it could conceivably produce eddies 1000 km large! This is truly remarkable.

But what to do about that energy? The energy after all is dissipated at the other end of the spectrum, at small scales. Presently we have no means to remove energy at large scales. So the energy will just pile up there, and the spectrum will never reach a steady state.

To avoid this, we require dissipation which acts at large scales. A good candidate is *Ekman friction*, which acts equally at all scales. As seen previously,[8] we can include Ekman friction by adding a linear term in the vorticity equation. Specifically, we modify (85) thus:

$$\frac{\partial}{\partial t}\zeta + \vec{u}\cdot\nabla(\zeta + f) = \mathcal{F} - r\zeta + \nu\nabla^2\zeta \tag{105}$$

where $\mathcal{F}$ is the forcing and where

$$r = \frac{f\delta_E}{2H}$$

is the inverse of the Ekman spin-down time. Here H is the depth of the fluid and δ_E is the Ekman layer thickness.

To see that Ekman friction acts equally at all scales, consider the case without forcing or small scale dissipation, with $f = const$. Then:

$$\frac{d}{dt}\zeta = -r\zeta \tag{106}$$

The solution to this is:

$$\zeta(t) = \zeta(0)e^{-rt} \tag{107}$$

So the vorticity decays exponentially, regardless of the scale.

Where does Ekman friction terminate the upscale cascade? As before, we equate time scales. The Ekman damping time scale is just r^{-1}. The advection time scale in the energy cascade is:

$$\tau \propto \epsilon^{-1/3}\kappa^{-2/3}$$

Equating them, we can solve for the large scale dissipation wavenumber:

[8] See the notes from GEF2220 and GEF4500.

$$\kappa_r = (\frac{r^3}{\epsilon})^{1/2} \tag{108}$$

This is the boundary between the energy inertial range and the largest scales, which are dominated by Ekman friction.

Now to the other inertial range. This is where enstrophy cascades down-scale, to smaller scales. In analogy to the energy range, here we have an enstrophy cascade rate, η. From the enstrophy equation, we know the enstrophy transfer has units of $1/T^3$, as the enstrophy has units of $1/T^2$. From dimensional grounds, we infer the spectrum has a shape:

$$E(\kappa) = C\eta^{2/3}\kappa^{-3} \tag{109}$$

So this is steeper than the energy inertial range.

An interesting thing about the enstrophy cascade range is that, unlike with the energy inertial range, the advective time scale is *independent of the length scale*. We have simply that:

$$\tau \propto \eta^{-1/3} \tag{110}$$

In fact, this time scale is determined by the largest eddies in the cascade range. The enstrophy cascade is essentially non-local—the smaller scales are stirred by the eddies at the top of the inertial range.

Equating this time scale with the dissipation time at small scales, $\tau_d = (\nu\kappa^2)^{-1}$, we get the dissipation wavenumber:

$$\kappa_\nu = (\frac{\eta^{1/3}}{\nu})^{1/2} \tag{111}$$

This is where the enstrophy cascade terminates. We can calculate the rate at which enstrophy is dissipated by scaling the enstrophy equation (63). At

the dissipation scale, the RHS of (63) scales as:

$$\nu \left|\nabla \times \zeta\right|^2 \propto \nu \frac{U^2}{L^4} \propto \nu \frac{\eta^{2/3}\kappa_\nu^{-2}}{\kappa_\nu^{-4}} = \nu \frac{\eta^{2/3}\eta^{1/3}}{\nu} = \eta \qquad (112)$$

So as with the energy cascade in 3-D turbulence, the enstrophy cascade is independent of the viscosity, ν. Even if ν is very small, enstrophy is transferred to the small scales to be dissipated. Thus enstrophy is *not* conserved in 2-D turbulence, since it will always (eventually) be dissipated.

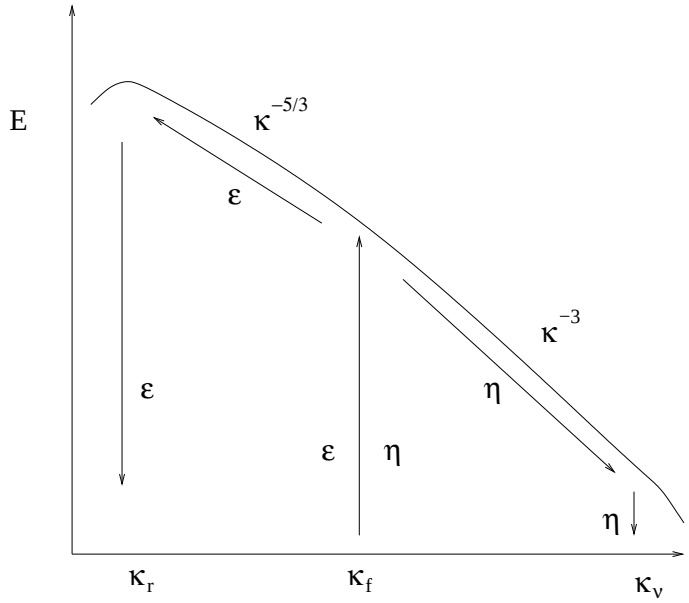

Figure 16: The energy spectrum for stationary 2-D turbulence, forced at wavenumber κ_f.

We summarize the cascades in Fig. (16). Energy and enstrophy are "injected" into the system at wavenumber κ_f. There are two inertial ranges: the $\kappa^{-5/3}$ range at larger scales and the κ^{-3} range at smaller scales. Energy cascades at a rate, ϵ, and enstrophy at a rate, η. Energy is removed at large scales by Ekman friction and at small scales by molecular dissipation.

Exercise: *Energy dissipation rate*

Check that the energy lost to Ekman damping at the upper limit of the

energy range is also equal to ϵ.

7.4 Physical interpretation

But what is enstrophy? How do we visualize these different cascades?

To see, it helps to understand the difference between the streamfunction and vorticity, and between energy and enstrophy. The vorticity is:

$$\zeta = \nabla^2 \psi$$

In terms of Fourier-transformed variables, we have:

$$\hat{\zeta} = -\kappa^2 \hat{\psi}$$

So the vorticity is multiplied by the wavenumber squared. That means that vorticity is like a high-pass filtered version of the streamfunction.

Shown in Fig. (17) is the streamfunction obtained from a 2-D turbulence simulation (run without forcing, from random initial conditions). The field is fairly smooth, with high and low pressure regions side by side. In the right panel is the vorticity field at the same time. This has much more small scale structure. There are vortices, but also many small filaments between the vortices. We could hardly have guessed these structures existed, looking at the streamfunction.

The energy essentially reflects the streamfunction, and the enstrophy the vorticity. From before, we showed that:

$$Z(\kappa) = \kappa^2 E \tag{113}$$

So the enstrophy is like a high-pass version of the energy. While the energy reflects the large scale structures, the high and low pressures in Fig. (17), the enstrophy is more affected by the small scale filaments being strained

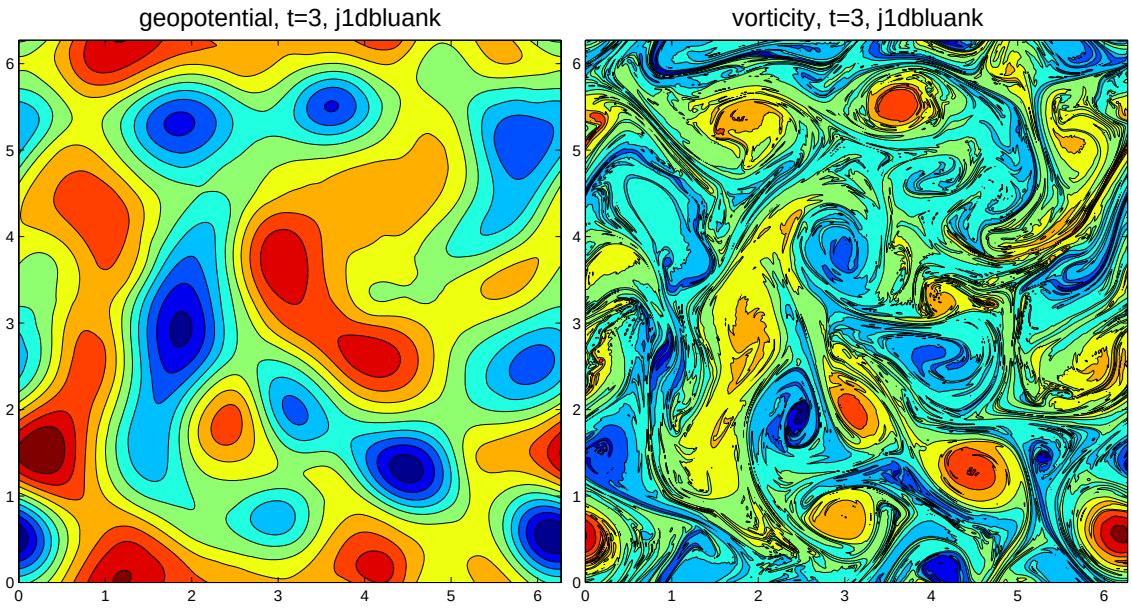

Figure 17: A snapshot of the streamfunction (left) and vorticity (right) from a 2-D turbulence simulation. Note the vorticity has much more small scale structure.

out *between* the pressure systems. It is these filaments which are being dissipated by the small scale damping.

7.5 The vortex view

The tradition view of 2-D turbulence, following Kraichnan (1967), is in terms of the Fourier components. Like Kolmogorov (1941), we have assumed the turbulence is homogeneous and isotropic. But as with the velocity gradients in 3-D turbulence, 2-D turbulence exhibits intermittency. And this intermittency is hard to miss— if one looks at the vorticity field.

Beginning in the 1980s, the computer power was sufficient to simulate 2-D turbulence at reasonably large Reynolds numbers. What researchers began to see was that the vorticity is dominated by long lived or "coherent" vortices. These are essentially the cyclones (and anticyclones) which are familiar in the weather. Atmospheric vortices also persist for long periods

of time—it is possible to track storms from their origin in the western Atlantic to their demise in the Nordic Seas.

Vortices also account for *extreme* velocities. An observer at a fixed location will notice the velocities rise and fall, then a vortex will strike and the velocities will be very large, as with a hurricane. Having vortices also mean the flow is no longer homogeneous—the vortex parts of the flow are distinct from other locations.

In two seminal papers, McWilliams (1984, 1990) noticed that freely-evolving (unforced) turbulence quickly evolves to a state where the vortices dominate the flow, as the vorticity between vortices is strained out and dissipated. Thereafter, the evolution is primarily a process of *mergers* between vortices. Positive vortices (cyclones) merge with other cyclones and negative vortices (anticyclones) merge with other anticyclones. The merged vortices are larger than the vortices which joined to make them. In this way, energy is shifted toward larger scales—the flow is dominated by fewer, larger vortices.

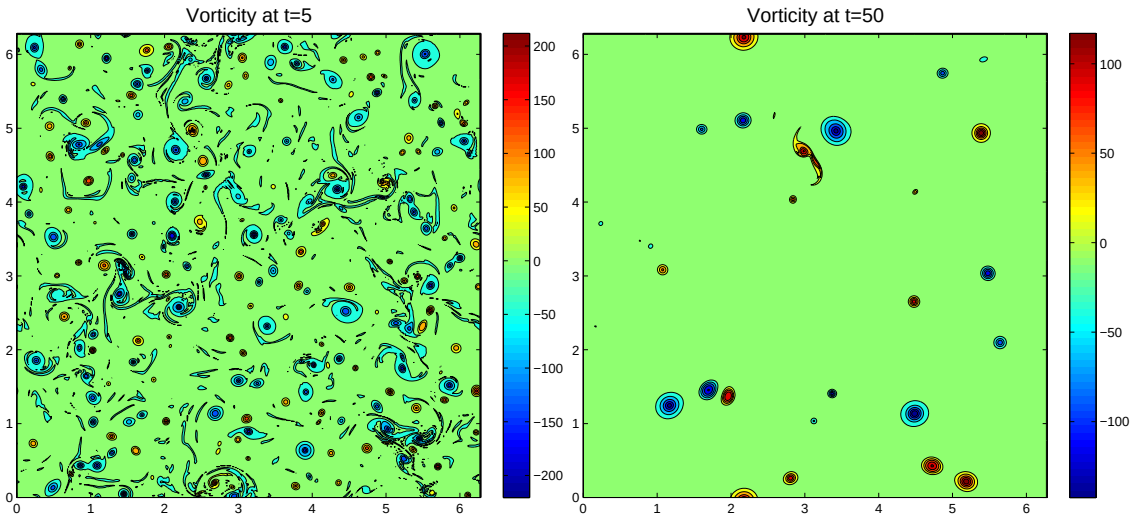

Figure 18: Snapshots of the vorticity from a 2-D turbulence simulation. The panel at left is at an earlier time, and the one at right at a later time.

This is illustrated in Figs. (18). The left panel shows the vorticity from a simulation begun with random initial conditions. After a short period, vortices emerge, with both signs (cyclones and anticyclones). As time goes by, the vortices merge, so there are fewer at later times (right panel). Left to itself, the system would eventually evolve to a dipole—one cyclone and one anticylcone.

McWilliams (1990) studied the statistics of the vortices. He found that the number of vortices decays as a *power law* (Fig. 19), i.e.:

$$N_v \propto t^{-\alpha} \tag{114}$$

where $\alpha \approx 0.7$. The finding was supported in a subsequent calculations using "point vortices" (right panel of Fig. 19).

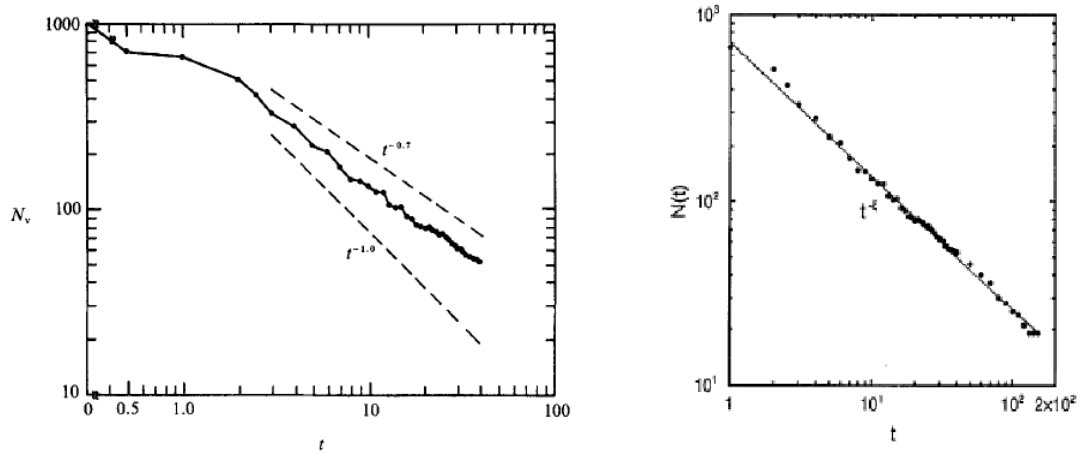

Figure 19: The number of vortices as a function of time for a freely-evolving turbulence simulation (left panel); from McWilliams (1990). The number of vortices in a "point vortex" simulation (right panel); from Weiss and McWilliams (1993).

The vortices are important for the flow. Carnevale et al. (1991) showed that all the important measures in these simulations could be explained in terms of the vortex statistics. Theirs is a "mean field theory", and it goes as

follows. Assume that the vortices are *patches* of uniform vorticity, positive or negative. Thus the vorticity of a vortex can be written:

$$\zeta = \begin{cases} \zeta_c & \text{if } r \leq b \\ 0 & \text{if } r > b \end{cases}$$

Here b is the radius of the vortex patch.

The patch also has a velocity field. Using cylindrical coordinates and assuming no radial flow, we have:

$$\zeta = \frac{1}{r}\frac{\partial}{\partial r}(rv) \tag{115}$$

So:

$$v = \frac{1}{r}\int_0^r \zeta r \, dr \tag{116}$$

Thus for the patch:

$$v = \begin{cases} \zeta_c r/2 & \text{if } r \leq b \\ \zeta_c b^2/(2r) & \text{if } r > b \end{cases}$$

Using this, we can calculate the energy of the vortex. Integrating over the domain (which we assume is larger than the vortex radius, b), we get:

$$E = \frac{1}{L^2}\int_0^L \frac{v^2}{2} r \, dr = C\zeta_c^2 b^4 \tag{117}$$

where C is a constant which depends on the domain scale, L (we've assumed a square domain here, for simplicity).

If there is more than one vortex, the total energy is the sum of the contributions from all the vortex patches:

$$E = \sum_i E_i \tag{118}$$

We will neglect the energy associated with the integrations between the vortices. To write this sum, we make a mean field approximation; we have replace the sum above with N times the average vortex quantities, if N is the total number of vortices. Thus we have:

$$E \propto \frac{1}{L^2} NC\, \zeta_c^2\, b^4 \propto \rho\, \zeta_c^2\, b^4 \tag{119}$$

where ρ is the vortex density in the domain, N/L^2.

Now, we demand that energy be conserved in this system—so E =const. Thus:

$$\rho\, \zeta_c^2\, b^4 = const. \tag{120}$$

We know that:

$$\rho \propto t^{-\alpha} \tag{121}$$

with $\alpha \approx 0.7$. This means that the product of $\zeta_c^2\, b^4$ must *increase* at the same rate.

Carnevale et al. make one further assumption—that the vortex amplitude is also conserved in mergers. If we take two patches and combine them, the amplitude won't change. That implies that the mean amplitude is also constant. So:

$$b \propto t^{\alpha/4} \tag{122}$$

The mean vortex radius is growing in time. Likewise, the mean area is also growing:

$$A = \pi b^2 \propto t^{\alpha/2} \tag{123}$$

This is the inverse cascade in the model—mergers are producing larger and larger vortices.

Interestingly, the vortex mergers do *not* conserve enstrophy. The enstropy for a single vortex is:

$$Z = \frac{1}{L^2} \iint \zeta^2 \, dA = \frac{1}{L^2} \zeta_c^2 \pi b^2 \tag{124}$$

because the vorticity is constant inside and zero outside the patch. Again the total enstrophy is the sum over all the patches:

$$Z = \sum_i Z_i = \frac{1}{L^2} N \; \zeta_c^2 \, \pi \, b^2 \propto \rho \, \zeta_c^2 \, b^2 \tag{125}$$

Thus we have that:

$$Z \propto t^{-\alpha} \, t^0 \, t^{\alpha/2} = t^{-\alpha/2} \tag{126}$$

Given McWilliams' value for $\alpha = 0.7$, this implies the enstrophy decays as $t^{-0.35}$. This is remarkable, because except for the mergers, this vortex patch system has *no dissipation* at all. The prediction was supported by numerical simulations (Fig. 20).

Why does enstrophy decrease? During mergers, small *filaments* are cast off. These are then assumed to be dissipated by small scale damping. The mergers thus conserve energy, but they don't conserve vorticity.

The vortex view of 2-D turbulence is that the dynamics are determined by the vortices. Vortex mergers conserve energy, but enstrophy decreases in time, as filaments are cast off. This is basically the same conclusion that we reached in discussing the inertial ranges. But the vortex view is an appealing physical description which is easy to grasp. We'll return to the mean vortex model later on.

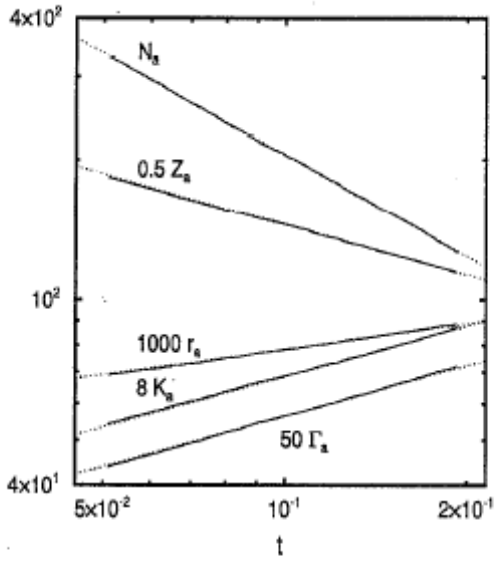

FIG. 10. A comparison of average vortex number $N_a(t)$, vortex radius $r_a(t)$, vortex circulation magnitude $\Gamma_a(t)$, enstrophy $Z_a(t)$, and kurtosis $K_a(t)$ from the modified point-vortex model (solid lines) and scaling theory (dotted lines). In the model, $t_0 < t < t_0 + t'_{end}$, where $t_0 = 0.050$ and $t'_{end} \approx 0.14$ is the earliest time for one of the 30 cycles to reach $N = 100$.

Figure 20: Vortex statistics from the simulations of from Weiss and McWilliams (1993). Here N, r and Γ are the vortex number and their mean radius and circulation. Z is the enstrophy and K is the vorticity kurtosis. The predictions from the mean vortex theory are indicated by lines.

Exercise: *Enstrophy conservation*

What if vortex mergers conserved enstrophy instead of energy? Show that in this case, the total energy would *grow* in time. Thus the two quantities cannot be simultaneously conserved in this model.

7.6 Passive tracer spectra

Thus far, we have focused on vorticity, which is an *active* tracer. Advection of an active tracer changes the flow. Thus momentum, density and vorticity are active tracers. But we can also ask what happens to a *passive* tracer, which has no affect on the flow. Examples are smoke, ash from volcanic

plumes and spilled oil. Temperature is often considered to be a passive tracer, but since it affects the density, it is actually an active one.

The equation for a passive tracer can be written thus:

$$\frac{\partial}{\partial t}C + \vec{u} \cdot \nabla C = \kappa \nabla^2 C \tag{127}$$

So time changes in the tracer occur because of advection, or by diffusion. The coefficient, κ, is the *diffusivity*. This is usually different from the viscosity, which dictates how molecular mixing affects the velocity. The main difference between this equation and that for momentum is that the tracer concentration, C, does not affect the velocity. So the advection term is *linear*. This is why the tracer is "passive".

Just as with energy and vorticity, we can speak of a spectra of the passive tracer. We can in particular talk about the tracer variance— the variation about the mean. If we Fourier transform, we can consider the tracer fluctuations as a function of scale—exactly as we do with enstrophy (the vorticity variance) or energy (the velocity variance).

What would such a spectrum look like? Following our previous arguments, we might expect that in a turbulent inertial range, the flux of tracer variance across scales will be constant. Otherwise the tracer variance would pile up at a certain scale (so we'd see filaments of a certain width emerging in the flow). The flux of volcanic ask would have units of concentration of ash squared per second. Let's call this flux χ.

Now the spectrum of tracer, $P(\kappa)$ will have units of tracer squared times length (so that the integral over all wavenumbers will yield tracer squared). So, on dimensional grounds, we expect:

$$P = \frac{\chi\tau}{\kappa} \tag{128}$$

where τ is the turbulent time scale.

Here is where the passive element comes in. The tracer doesn't affect the time scale, τ; that only depends on the active portion of the flow, the vorticity. So for τ, we will use the time scales inferred for the turbulent ranges.

For the energy range, $\tau = \epsilon^{-1/3}\kappa^{-2/3}$. Substituting in, we get:

$$P(\kappa) = \chi\epsilon^{-1/3}\kappa^{-5/3} \tag{129}$$

So in the energy range, the tracer spectrum has the same slope as the energy spectrum.

For the enstrophy range, we have $\tau = \eta^{-1/3}$. As noted, the enstrophy range is "non-local" because the time scale is set by the largest eddies in the range (as opposed to a "local" range, where the time scale is determined by the eddies which have the same size). Substituting in, we get:

$$P(\kappa) = \chi\eta^{-1/3}\kappa^{-1} \tag{130}$$

So the spectra is shallower than the energy spectrum. Interestingly though, the tracer spectrum is the *same* as the enstrophy spectrum (see below). This implies that vorticity is advected in the enstrophy range *like a passive tracer*, even though it is an active tracer. The reason is that the enstrophy range is non-local; all fields are advected passively by the largest eddies in the range.

The spectra are summarized in Fig. (21). We assume that tracer is being put in at the largest scales. Tracer variance then cascades *downscale*,

through both the energy and enstrophy ranges. The spectral slopes are $\kappa^{-5/3}$ and κ^{-1}.

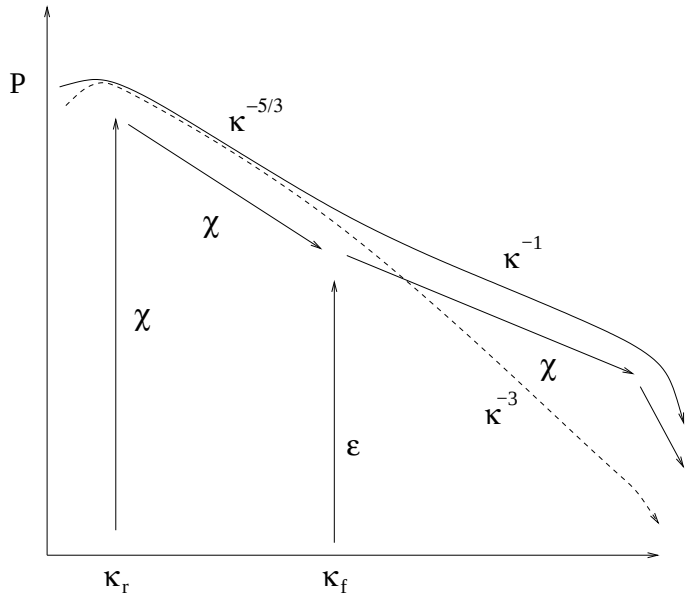

Figure 21: The passive energy spectrum in forced 2-D turbulence. The forcing is applied at κ_f, and the tracer is introduced at large scales, at κ_χ. Note the tracer variance cascades downscale at all scales.

Exercise: *Enstrophy spectrum*

Derive the enstrophy spectrum in the two inertial ranges for 2-D turbulence. Show then that the slope in the enstropy range is the same as that for a passive tracer.

7.7 Predictability

Another interesting application of turbulence phenomenology is to predictability. Imagine the atmosphere was really just a 2-D turbulent fluid. Now consider that there is an error in the initial conditions at some small scale. We know the winds at large scales, from measurements, but we can't know them precisely at, say, the 1 meter scale. Because the atmosphere is

chaotic, these slight differences in the modelled initial state and the actual state will grow, eventually disturbing the forecasts at large scales. But how quickly will this happen?

7.7.1 Lorenz Model

The usual point of reference for atmospheric predictability is Lorenz's (1963) model. This model is essentially a *three mode truncation* of the equations describing a convective fluid system, under the influence of heating of the lower boundary. In other words, we Fourier transform the variables and only retain three terms. His equations can be written:

$$\begin{aligned} \frac{dx}{dt} &= \sigma(y - x) \\ \frac{dy}{dt} &= rx - y - xz \\ \frac{dz}{dt} &= xy - bz \end{aligned} \tag{131}$$

Here x, y, z are "state variables", representing temperature and velocity in the convective system, and where σ, r, b are various parameters. The equations are nonlinear, due to the xz and xy terms in the second and third equations. As with the logistic map (sec. 4), these terms are the source of the system's unpredictability.

The equations have three fixed points:

$$(x, y, z) = (0, 0, 0), \quad (a, a, r - 1), \quad (-a, -a, r - 1) \tag{132}$$

Here

$$a = \sqrt{b(r - 1)}$$

The first solution is the trivial one, with no motion. The other two have convection, with opposing circulation.

If you integrate the equations numerically, you find that the system orbits around one of the two non-trivial fixed points for a while, then abruptly makes a transition to orbit around the other. These transitions are unpredictable. And as with the logistic map, the system exhibits a sensitive dependence on the initial condition.

Predictability is a measure of how quickly the system diverges under a change in the initial condition. In the Lorenz model, the error growth depends on where the system is in phase space, i.e. in (x, y, z) space. But the error generally grows *exponentially* in time, and the magnitude of the error depends on that of the initial condition. So the smaller the initial error, the longer it takes for the error to propagate through the system.

However, the Lorenz model isn't very realistic. Think if we truncated our turbulence model with only three wavelengths. Energy could pass from to the other, but it couldn't go any further. Thus energy would have to recycle between the three wavenumbers.

7.7.2 Predictability in 2-D turbulence

As we've seen, the actual turbulence system has a huge range of accessible wavenumbers. Furthermore, our turbulence can be forced, and it can acquire a statistically stationary state. There is no forcing or dissipation in the Lorenz model, so it is never in a steady state; energy continually moves back and forth between scales.

So how do errors propagate through a turbulent system? [9] If the cascade

[9]The researcher C. Leith from the National Center for Atmospheric Research (NCAR) was an early proponent of using turbulence models to understand predictability. The following section is based on the presentation in Vallis's book, *Atmospheric and Oceanic Fluid Dynamics.*

is *local*, an error at one scale would affect the next largest scale. Then that scale would affect the next scale, and so on up to the largest scales. The total time to reach the largest scale would then be an integral over all wavenumbers.

To express this mathematically, we can speak of a "spectrum" of interaction times:

$$P = \frac{\tau(\kappa)}{\kappa} \tag{133}$$

Again we divide by κ so that the integral over all wavelengths will produce a quantity with units of time, i.e.:

$$T = \int_{\kappa 0}^{\kappa 1} \frac{\tau}{\kappa}\, d\kappa \tag{134}$$

Here κ_1 is the scale where the error is introduced, and κ_0 is our "weather scale", the large scale we're focused on.

Consider the enstrophy cascade first. Here $\tau = \eta^{-1/3}$, so:

$$T = \int_{\kappa 0}^{\kappa 1} \frac{\eta^{-1/3}}{\kappa}\, d\kappa = \eta^{-1/3}\, ln(\frac{\kappa_1}{\kappa_0}) \tag{135}$$

The predictability time depends on the scale of the error, so we can increase the predictability time by reducing the scale of the error (increasing κ_1). In addition, the errors grow exponentially in time. Rewriting the equation in terms of scales, $L \propto \kappa^{-1}$, we get:

$$L_0 = L_1\, e^{\eta^{1/3} T} \tag{136}$$

So scale of the error increases with a rate proportional to $\eta^{1/3}$. Thus the enstrophy range is in line with our expectations from the Lorenz model.

Now consider the energy inertial range. Then $\tau = \epsilon^{-1/3}\kappa^{-2/3}$. Substituting in, we get:

$$T = \int_{\kappa 0}^{\kappa 1} \epsilon^{-1/3}\kappa^{-5/3}\, d\kappa \propto \epsilon^{-1/3}\kappa^{-2/3}|_{\kappa 0}^{\kappa 1} \tag{137}$$

Now if the scale of the error is much smaller than the largest eddies, we have:

$$T \approx \epsilon^{-1/3}\kappa_0^{-2/3} \tag{138}$$

Thus with an energy cascade, the predictability time is *independent* of the scale of the error! This is quite different from the Lorenz model. The reason is that in the energy cascade the interaction time decreases with increasing wavenumber. So the error propagation depends on the largest scales, where the error transfer is the slowest.

7.7.3 Predictability in the atmosphere

Given these ideas, what would we infer about the atmosphere. To know that, we need an idea of the energy spectra. Nastrom and Gage (1985) used velocity data collected from over 6000 commercial aircraft to calculate wavenumber spectra. The spectra are shown in Figure (22). These indicate a κ^{-3} range from 100-2000 km and a $\kappa^{-5/3}$ range at smaller scales. The κ^{-3} range is thought to be en enstrophy cascade (e.g. Lindborg, 1999). The dynamical basis of the $\kappa^{-5/3}$ range is still debated. If it is a 2-D energy cascade, it implies a source of energy at small scales. The scales are somewhat too large to be a 3-D energy range, but some have argued for that. Others have suggested it is due to temperature anomalies on the tropopause (Tulloch and Smith, 2006). Whatever the case, the small scale

range is *local*.

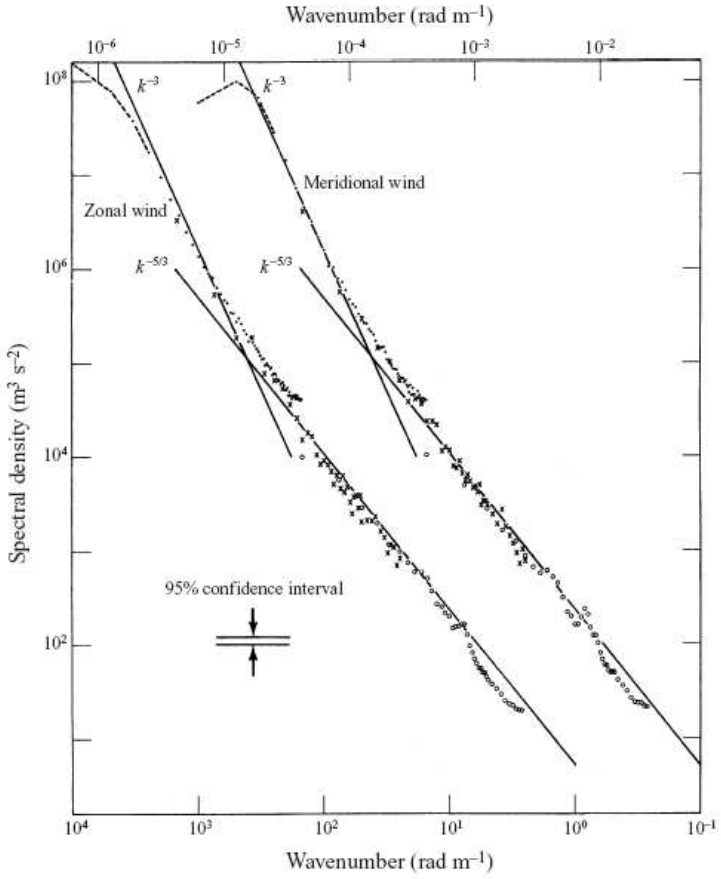

Figure 22: Kinetic energy spectra from data collected on commercial airplanes over the U.S. The zonal and meridional components are shown, with the latter shifted one decade to the right. Note the lower x-axis is mislabeled— it should say "wavelength". From Nastrom and Gage (1985).

Given what we now know about 2-D turbulence, we infer that the predictability is limited by the local range at small scales, and by the transition scale, 100 km. The latter would determine κ_0 in the previous discussion. So regardless of how good our observations are, we could not improve the predictability time. Using approximate values for the dissipation rate, we obtain a value of T on the order of a week. We caution though that the dissipation rate is not well-known; indeed, even its sign is debated in the

smaller scale range.

8 Geostrophic turbulence

Figure (22) raises some interesting questions though. The two dimensional system we have considered so far is very idealized. The flow in the atmosphere and ocean are affected by planetary rotation, stratification and bottom topography, to name only a few complicating factors. Yet we still see energy spectra which resemble those in pure 2-D turbulence. How can this be?

Geostrophic turbulence is what happens when we add these more realistic factors. The name comes from an article (Charney, 1971) where two dimensional turbulence was considered in a quasi-geostrophic fluid with continuous stratification. But we use the term to also encompass variations in f and in topography. We begin with f.

8.1 The Beta-effect

The vorticity equation (61) in two dimensions is given by:

$$\frac{\partial}{\partial t}\omega + \vec{u} \cdot \nabla \omega_a = \nu \nabla^2 \omega \tag{139}$$

Using only the vertical component of the vorticity, this is:

$$\frac{\partial}{\partial t}\zeta + \vec{u} \cdot \nabla (\zeta + f) = \nu \nabla^2 \zeta \tag{140}$$

Before we assumed that f was constant, so that it drops out of the vorticity equation completely. Thus a constant Coriolis parameter has no effect on 2-D turbulence.

Now let's examine what happens when f varies with latitude. For this, we will use the *Beta-plane approximation*. Specifically, we Taylor-expand the Coriolis parameter about a central latitude, θ_0:

$$f(\theta) = f(\theta_0) + \frac{df}{d\theta}(\theta_0)\ (\theta - \theta_0) + \frac{1}{2}\frac{d^2 f}{d\theta^2}(\theta_0)\ (\theta - \theta_0)^2 + ... \qquad (141)$$

We neglect the higher order terms, so that:

$$f \approx f(\theta_0) + \frac{df}{d\theta}(\theta_0)\ (\theta - \theta_0) \equiv f_0 + \beta y \qquad (142)$$

where

$$f_0 = 2\Omega sin(\theta_0)$$

$$\beta = \frac{1}{a}\frac{df}{d\theta}(\theta_0) = \frac{2\Omega}{a}cos(\theta_0)$$

and

$$y = a(\theta - \theta_0)$$

Here a is the radius of the earth.

Substituting this into the vorticity equation, and neglecting the dissipation for the moment, we obtain:

$$\frac{\partial}{\partial t}\zeta + \vec{u} \cdot \nabla\zeta + \beta v = 0 \qquad (143)$$

The fundamental difference here is that meridional motion can induce changes in the relative vorticity. This can be seen clearly if we rewrite the equation in Lagrangian form:

$$\frac{d}{dt}(\zeta + \beta y) = 0 \qquad (144)$$

This implies:

$$\zeta + \beta y = const. \tag{145}$$

for a parcel. If the parcel moves north, to greater y, it's vorticity must decrease. As such, the β-effect *constrains* North-South motion.

The linear version of the vorticity equation is just:

$$\frac{\partial}{\partial t}\zeta + \beta v = 0 \tag{146}$$

Written in terms of the 2-D streamfunction, this is:

$$\frac{\partial}{\partial t}\nabla^2\psi + \beta\frac{\partial}{\partial x}\psi = 0 \tag{147}$$

Substituting a wave solution:

$$\psi = \hat{\psi}\, e^{ikx+ily-i\omega t} \tag{148}$$

we obtain:

$$\omega = -\frac{\beta k}{k^2 + l^2} \tag{149}$$

which is the dispersion relation for *Rossby waves*. Rossby waves, discovered by C. G. Rossby (1936) are fundamental to our understanding of time variability in the atmosphere.

Rossby waves have a zonal phase speed of:

$$c_x = \frac{\omega}{k} = -\frac{\beta}{k^2 + l^2} \tag{150}$$

So Rossby waves always propagate to the west (in the absence of a mean flow) and larger waves move faster than smaller waves.

Now let's put advection back into the problem. Now we expect that the flow can also be turbulent. But which scales are turbulent and which are wave-like? We can get a rough idea by simply scaling the vorticity equation:

$$\frac{\partial}{\partial t}\zeta + \vec{u}\cdot\nabla\zeta + \beta v = 0$$

$$\frac{U}{LT} \qquad \frac{U^2}{L^2} \qquad \beta U$$

$$\frac{1}{\beta LT} \qquad \frac{U}{\beta L^2} \qquad 1 \tag{151}$$

Recall that the vorticity scales as U/L. In the last line, we've divided through by βU. We see that the advective term scales as $U(\beta L^2)^{-1}$. This is essentially the Rossby number, if we substitute $f \approx \beta L$.

If this parameter is small, the equation should be approximately linear and the flow will be dominated by Rossby waves. If it is large, the β term will be unimportant and the dynamics will be turbulent.

Thus we expect a "boundary" between wave and turbulent dynamics, with the latter occurring at small scales and the former at larger scales. The separation scale is often called the "Rhines scale" after Rhines (1975):

$$L_\beta = \sqrt{\frac{U}{\beta}} \tag{152}$$

At L_β, all three terms in the vorticity equation are of equal importance.

Note we haven't specified a time scale in the vorticity equation. This is because we assume the time scale adjusts to the dynamics. With Rossby waves, the first term should balance the third, so that $T = (\beta L)^{-1}$. If turbulence, we would expect the advective time scale, $T = L/U$.

Imagine we have a source of energy at some small scale L_f (our "spoon", stirring the fluid). This will generate a cascade to larger scales. But at some scale, Rossby waves will dominate over turbulence. At these scales, the dynamics will be quasi-linear and turbulent transfers will be weak or non-existent. So we expect that β will halt or *arrest* the cascade. At what scale does this occur?

An interesting thing happens though when you run a numerical simulation of this. An example is shown in Fig. (23), of simulations with a barotropic fluid on a sphere. Recall that a sphere is periodic in the x direction. The simulations show the energy cascade does indeed arrest, but the arrest is *anisotropic*) in that the flow develops zonal jets. The result is a banded structure, reminiscent of the Jovian atmosphere.

The anisotropy comes about because the Rossby wave dispersion relation is also anisotropic—there is a k in the numerator, but no l. As such, different scales of motion have different wave periods, depending on their zonal and meridional extent. If we write the wave time scale as:

$$\tau_\beta \propto |\omega^{-1}| = \frac{k^2 + l^2}{\beta k} \tag{153}$$

we see that the time scale increases *without bound* as $k \to 0$. Zonal jets have $k = 0$.

We can re-write the wave time in terms of the total wavenumber vector, κ:

$$\tau_\beta = \frac{\kappa^2}{\beta \kappa cos(\theta)} = \frac{\kappa}{\beta cos(\theta)} \tag{154}$$

Here θ is the angle the wavevector makes, i.e.:

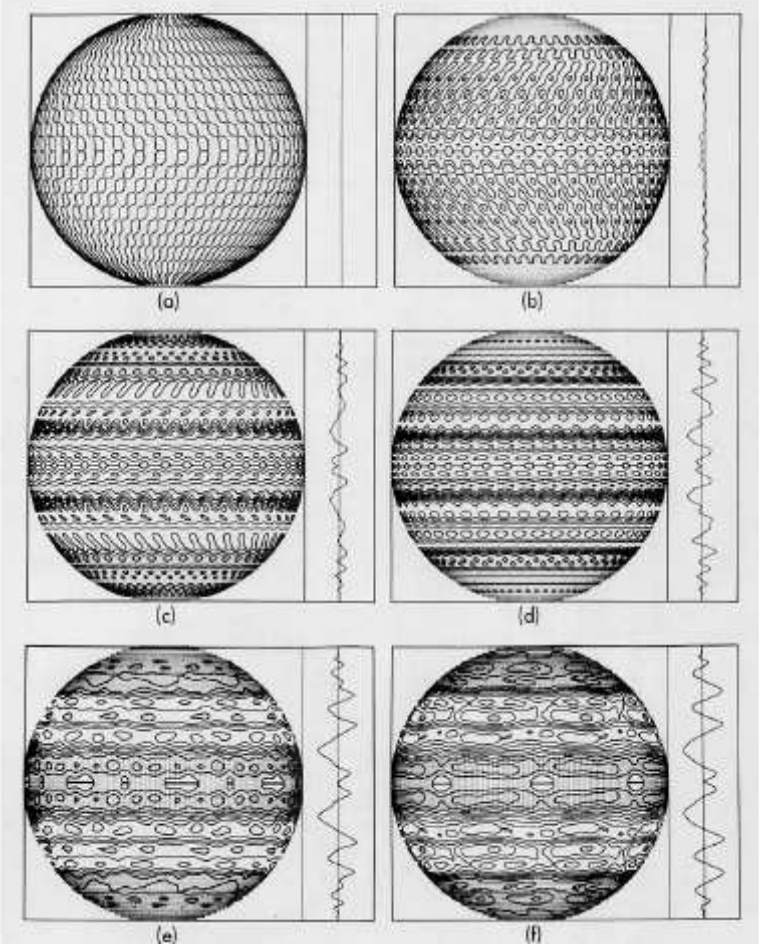

Figure 23: Numerical simulations of forced barotropic turbulence on a sphere. Note the formation of banded flow, superimposed over a field of eddies. The mean zonal velocities are indicated in the inserts. From Williams (1978).

$$(k, l) = [\kappa cos(\theta), \kappa sin(\theta)] \tag{155}$$

At the transition from turbulence to Rossby waves, the wave time scale equals the turbulent time scale. In the energy cascade, this is:

$$\tau = \epsilon^{-1/3} \kappa^{-2/3} \tag{156}$$

The two time scales are equal when:

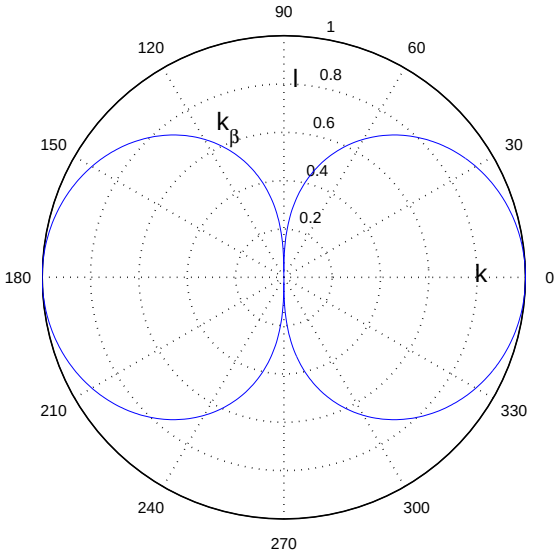

Figure 24: The boundary between turbulence and Rossby waves. For plotting, we assume $\beta^3/\epsilon = 1$.

$$\epsilon^{-1/3}\kappa^{-2/3} = \frac{\kappa}{\beta cos(\theta)} \tag{157}$$

or:

$$\kappa \equiv \kappa_\beta = (\frac{\beta^3}{\epsilon})^{1/5} cos^{3/5}(\theta) \tag{158}$$

(Vallis and Maltrud, 1993). This has two components:

$$(k_\beta, l_\beta) = [(\frac{\beta^3}{\epsilon})^{1/5} cos^{8/5}(\theta), (\frac{\beta^3}{\epsilon})^{1/5} cos^{3/5}(\theta) sin(\theta)] \tag{159}$$

The result is an arrest *boundary* in (k, l) space. The boundary is plotted in Fig. (24). It has two symmetric lobes. Outside the lobes, the wavenumbers are participating in triad interactions and moving energy toward the lobes. Inside the lobes, the dynamics are essentially linearly and the energy flux is weak.

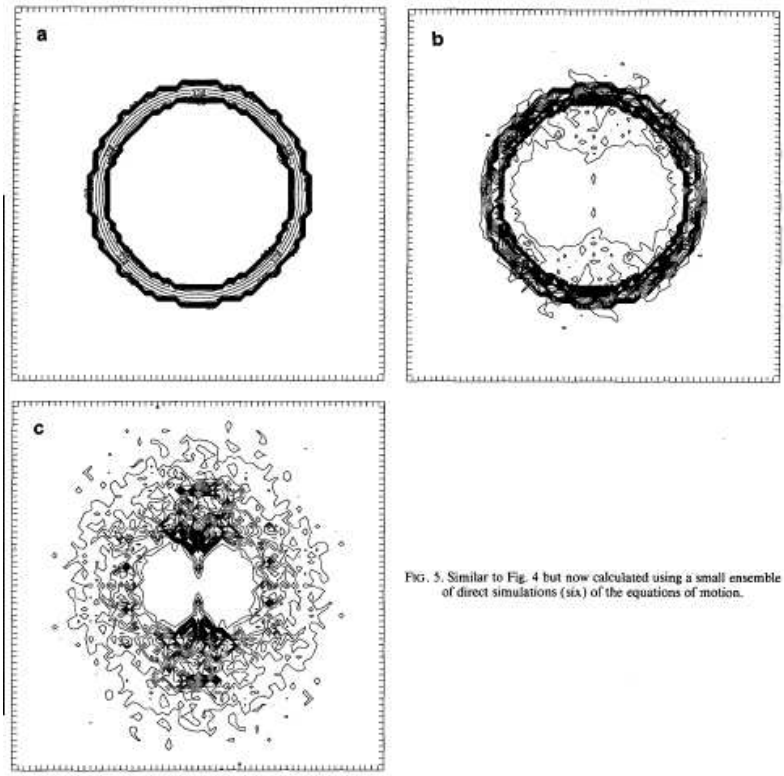

FIG. 5. Similar to Fig. 4 but now calculated using a small ensemble of direct simulations (six) of the equations of motion.

Figure 25: Spectra from a freely-evolving 2-D turbulence simulation, plotted in wavenumber space. From Vallis and Maltrud (1993).

Vallis and Maltrud (1993) tested this prediction with numerical simulations. They employed a 2-D model, with random initial conditions. The latter were isotropic and covered a specified band in wavenumber space (upper left panel of Fig. (25). The initial spectrum thus appears as a ring in $(k.l)$ space. As time proceeds, energy spreads inward, shifting toward smaller wavenumbers. But it ceases at the lobe structures described above. Vallis and Maltrud called these "dumbbell" structures.

The "dumbbell" shape explains the anisotropy observed in Fig. (23). Consider energy moving in along the axis where $l = 0$ (the x-axis in the figure). The energy cascade here would stop at $k = 1$. But energy moving along the y-axis, with $k = 0$, will proceed nearly to the center. The reason

is that if $k = 0$, the meridional velocity is zero and the β term drops out of the vorticity equation. So for zonal motion, it is as if the β effect were non-existent.

This implies that a forced cascade with β will produce structures with $k = 0$—zonal jets—as in Fig. (23). But there are also eddies superimposed on the bands; this is the turbulence at smaller scales. The mean velocities indicate alternating eastward and westward flow. However that flow is asymmetric; the eastward jets are sharper than the westward ones. This is a consequence of barotropic stability, which favors sharper eastward jets.

Exercise: *Topographic arrest*

A bottom slope acts exactly like the β-effect in a barotropic fluid. The vorticity equation (see eq. 182 below) can be written:

$$\frac{\partial}{\partial t}\zeta + \vec{u} \cdot \nabla(\zeta + h) = 0 \tag{160}$$

where h is the topographic elevation. Say that $h = \alpha x$ (the bottom slopes up to the east). Find the dispersion relation for the waves (assume periodic boundary conditions in x and y). Now solve for the arrest wavenumber. Draw it in (k, l) space. What type of structures do you expect?

8.2 Beta turbulence in a closed basin

Zonal jets can exist in re-entrant domains, like the atmosphere. Indeed, the Jet Stream is a zonal jet, albeit a highly time-dependent one. But can such jets exist in the *ocean*, where there are lateral (continental) boundaries?

To see, we must consider Rossby waves in a closed basin. These have a slightly different structure and dispersion relation than the plane Rossby waves discussed above. The waves have a dual structure— a propagating

wave superimposed upon a stationary envelope. The latter ensures that there is no flow on the boundaries. For a rectangular basin, the streamfunction takes the form (e.g. Pedlosky, 1987):

$$\psi = Acos(kx - \omega t)sin(\frac{m\pi x}{L_x})sin(\frac{n\pi y}{L_y}) \tag{161}$$

Here L_x and L_y and the lengths of the domain in x and y. The two sine terms ensure that the streamfunction vanishes on the boundaries, and the wavelengths are quantized. This solution is referred to as a barotropic *basin mode*.

The dispersion relation for a basin mode is given by:

$$\omega = \omega_{mn} = -\frac{\beta}{2\pi(m^2/L_x^2 + n^2/L_y^2)^{1/2}} \tag{162}$$

This too is quantized, i.e. there are only discrete values of the frequency, corresponding to the discrete wavenumbers. The dispersion relation resembles the plane Rossby wave dispersion relation, except that there is no "k" in the numerator. This makes all the difference.

The time scale for basin modes is the inverse of the frequency, which we can write as:

$$\tau = \frac{\kappa}{\beta} \tag{163}$$

where $\kappa = 2\pi(m^2/L_x^2 + n^2/L_y^2)^{1/2}$ is the (quantized) total wavenumber. Equating this to the turbulent time scale in the energy range:

$$\epsilon^{-1/3}\kappa^{-2/3} = \frac{\kappa}{\beta} \tag{164}$$

yields:

$$\kappa_\beta = \beta^{3/5}\epsilon^{-1/5} \tag{165}$$

for the arrest wavenumber (LaCasce, 2002). The important thing here is that the wave-turbulence boundary with basin modes is *isotropic*. There is no reason to expect zonal jets.

Numerical simulations confirm this. Shown in Fig. (26) are the streamfunctions from two forced simulations, one in a periodic domain (left panel) and one with solid walls (right). The former shows zonally-elongated structures, spanning the domain. The closed basin simulation on the other hand has mostly isotropic eddies. The only place where the flow is zonally elongated is along the northern boundary (where in fact a stationary gyre develops; Fofonoff, 1954).

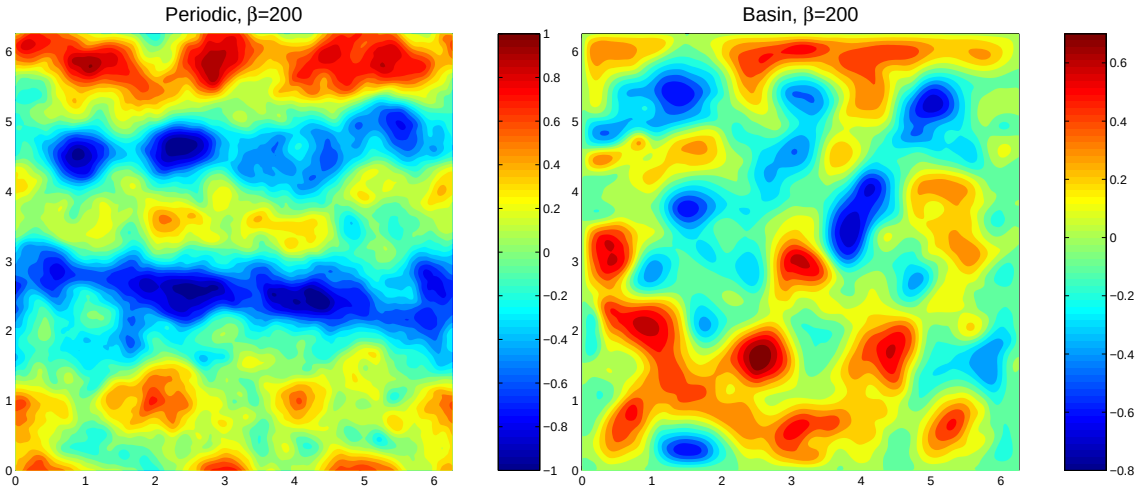

Figure 26: Streamfunctions from a forced 2-D turbulence simulations with periodic (left) and solid wall (right) boundary conditions.

We quantify the arrest further, as follows. In the simulations shown, the damping was with Ekman friction. The latter adds a term, $r\vec{u}$, to the RHS of the vector momentum equation. With this, the integrated energy equation (50) can be written:

$$\frac{d}{dt}E = \iiint \vec{u} \cdot \vec{\mathcal{F}}\, dV - r \iiint \vec{u} \cdot \vec{u}\, dV = \epsilon - 2rE \tag{166}$$

where E is the total kinetic energy. Notice that the forcing yields the energy flux, ϵ. In a statistically steady state, the LHS on average is zero, leaving:

$$\epsilon = 2rE \tag{167}$$

Using this, we estimate the arrest scale as:

$$L_\beta = \frac{2\pi}{\kappa_\beta} = 2\pi\beta^{-3/5}(2rE)^{1/5} \tag{168}$$

We compare this estimate to the simulations by calculating spatial correlations in the velocity field. In an eddy, the velocities are correlated (or anti-correlated) across the eddy. Outside the eddy, the velocities are uncorrelated with those in the eddy. So we can use velocity correlations to find the size of the eddies.

We plot the correlations as ellipses in Fig. (27). The solid and dashed curves correspond to two different ways of calculating the correlation (either using parallel velocities along a line—the longitudinal velocities—or perpendicular velocities—the transverse velocities). Both yield the same result; the eddy scales are isotropic and they are consistent with the length scale estimate in (168).

For comparison, the correlation ellipses from two simulations in a periodic domain are shown in Fig. (28). In this case, the longitudinal correlations (corresponding to the u velocities) are elongated in the x-direction. So this indicates large scale, coherent zonal flow. The transverse correlations on the other hand (corresponding to the v velocities in the x-direction)

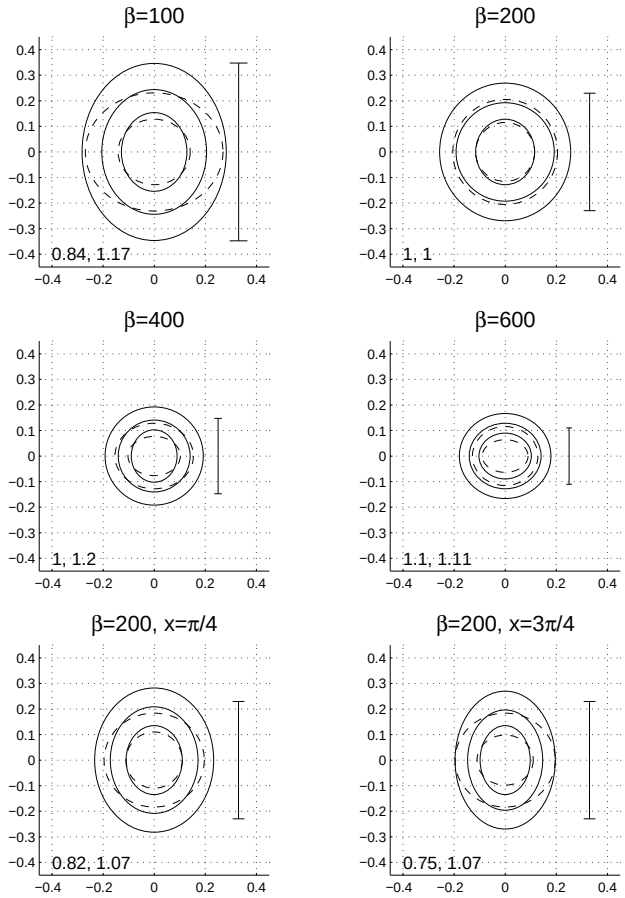

Figure 27: Velocity correlation ellipses from a series of experiments in a closed basin. The solid ellipses are from the longitudinal correlations (with values [0.8 0.6 0.4]); the dashed ellipses are transverse correlations (with values of [0.5 0]). The vertical lines indicate the arrest scale from (168). From LaCasce (2002).

are more nearly isotropic. These reflect the small scale eddies superimposed on the zonal jets.

Thus the arrest in a rectangular basin is similar to that described by Rhines (1975)—but it is isotropic. The isotropy stems from the fact that the wave time scale in a basin is also isotropic. So the boundaries prevent the formation of zonal jets. This example also highlights the importance of using time scales to understand how the turbulence behaves.

However, this case is still quite unrealistic in terms of the ocean, as the

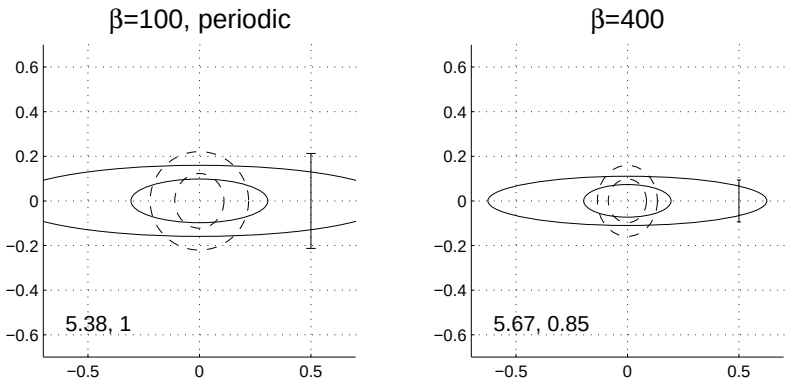

Figure 28: The velocity correlation ellipses from two simulations in a periodic domain. From LaCasce (2002).

bottom is entirely flat. The actual ocean of course has significant topography. We consider that next.

8.3 Topography

Bottom topography in a barotropic fluid acts very much like the β-effect. But instead of limiting N-S motion, topography inhibits motion *across the depth contours*. Thus an inverse cascade would be expected to generate jets over a topographic slope, exactly as seen in the last section. This was demonstrated by Vallis and Maltrud (1993).

But a major difference with topography is that it need not be a simple linear slope. We have mountains, ridges and closed basins. How would we expect such features to alter the inverse cascade?

This question was addressed in two independent, simultaneous papers—by Bretherton and Haidvogel (1976) and by Salmon, Holloway and Hendershott (1976). Both considered freely-evolving (unforced) turbulent flows over essentially any type of bottom topography. Salmon et al. used ideas from statistical mechanics to predict the most likely flow one would ex-

pect to find. Bretherton and Haidvogel used the calculus of variations. The two approaches are in fact related, as demonstrated later by Carnevale and Frederiksen (1987).

8.3.1 The barotropic vorticity equation

To do this problem, we require the vorticity equation for a barotropic fluid with variable depth. We obtain this as follows. Neglecting variations in f and forcing, the vorticity equation for a 2-D fluid is:

$$\frac{\partial}{\partial t}\zeta + \vec{u}\cdot\nabla\zeta + (\zeta + f_0)(\nabla\cdot\vec{u}) = \nu\nabla^2\zeta \tag{169}$$

We will assume that the velocities aren't purely 2-D, but that they are *quasi-geostrophic*. So the velocities are:

$$\vec{u} = (u, v, \epsilon w) \tag{170}$$

where ϵ, the Rossby number is small. So while not being exactly horizontal, the vertical velocity is much smaller. Note then that the continuity equation is:

$$\frac{\partial}{\partial x}u + \frac{\partial}{\partial y}v + \epsilon\frac{\partial}{\partial z}w = 0 \tag{171}$$

Furthermore, the vorticity is much smaller than f_0, because by scaling we have:

$$\frac{|\zeta|}{f_0} \propto \frac{U}{f_0 L} = \epsilon \tag{172}$$

Collecting these terms, we can write the vorticity equation thus:

$$\epsilon\frac{\partial}{\partial t}\zeta + \epsilon\vec{u}\cdot\nabla\zeta - (\epsilon\zeta + f_0)\epsilon\frac{\partial w}{\partial z} = \epsilon\nu\nabla^2\zeta \tag{173}$$

To first order in the Rossby number, this is:

$$\frac{\partial}{\partial t}\zeta + \vec{u}\cdot\nabla\zeta - f_0\frac{\partial w}{\partial z} = \nu\nabla^2\zeta \tag{174}$$

Now if the fluid is barotropic, there is no vertical shear.[10] As such, it is easy to integrate the equation over the depth of the fluid. Assume the lower boundary is at $z = -H(x, y)$ and that the upper boundary is a rigid surface, at $z = 0$. Then the integrated equation is:

$$H\frac{\partial}{\partial t}\zeta + H\vec{u}\cdot\nabla\zeta - f_0 w|_{-H}^{0} = H\nu\nabla^2\zeta \tag{175}$$

The vertical velocity at the upper boundary is zero. At the bottom, we can obtain w as follows. A parcel following the bottom has:

$$z = -H \tag{176}$$

Taking the Lagrangian derivative of both sides, we get:

$$w = -\frac{dH}{dt} = -\vec{u}\cdot\nabla H \tag{177}$$

To be consistent with the quasi-geostrophic approximation, we require that the bottom topography be small. So we write:

$$H(x, y) = D - h(x, y)$$

where

$$|h| \ll D \tag{178}$$

Using this in the integrated vorticity equation, we get:

[10] This is a consequence of the *Taylor-Proudman theorem*. See Pedlosky (1987) or my notes from GEF2220.

$$\frac{\partial}{\partial t}\zeta + \vec{u}\cdot\nabla\zeta + \frac{f_0}{H}\vec{u}\cdot\nabla h = \nu\nabla^2\zeta \tag{179}$$

or:

$$\frac{\partial}{\partial t}\zeta + \vec{u}\cdot\nabla(\zeta + \frac{f_0}{D}h) = \nu\nabla^2\zeta \tag{180}$$

Note too that the horizontal velocities are non-divergent to order Rossby number. So we can write the equation:

$$\frac{\partial}{\partial t}\zeta + \nabla\cdot[\vec{u}(\zeta + h)] = \nu\nabla^2\zeta \tag{181}$$

I've absorbed the factor of f_0/D into the topographic height, h, for simplicity. Lastly, we rewrite this in terms of the streamfunction, thus:

$$\frac{\partial}{\partial t}\nabla^2\psi + \nabla\cdot[\vec{u}(\nabla^2\psi + h)] = \nu\nabla^4\psi \tag{182}$$

This is the barotropic potential vorticity equation.

8.3.2 Conserved quantities

There are two conserved quantities in the limit of vanishing dissipation, i.e. $\nu \to 0$. One is the energy:

$$\frac{1}{2}\frac{\partial}{\partial t}\iint(u^2 + v^2)\,dxdy = 0 \tag{183}$$

The proof of this is left for an exercise. We also conserve "total enstrophy". First note that we can rewrite the vorticity equation (182) thus:

$$\frac{\partial}{\partial t}q + \nabla\cdot(\vec{u}q) = 0 \tag{184}$$

where

$$q \equiv \nabla^2 \psi + h \tag{185}$$

is the total vorticity. If we multiply the equation by q and integrate over space, we get:

$$\frac{\partial}{\partial t} \frac{1}{2} \iint q^2 \, dxdy + \iint \nabla \cdot (\vec{u} \, \frac{q^2}{2}) \, dxdy = 0 \tag{186}$$

The second term on the LHS is zero:

$$\iint \nabla \cdot (\vec{u} \, \frac{q^2}{2}) \, dxdy = \oint \frac{q^2}{2} \, \vec{u} \cdot \hat{n} \, dl \tag{187}$$

by Gauss' Law. This vanishes in a periodic domain or one with lateral walls.

So the total enstrophy, $q^2/2$, is also conserved. We will call this Q. Note though that the enstrophy itself is *not* conserved. This is because the interaction with the topography itself can produce enstrophy.

Exercise: *Energy conservation*

Prove that the integrated kinetic energy is conserved, starting directly with the vorticity equation (182), if $\nu = 0$.

8.3.3 Minimum enstrophy

Under a dual cascade scenario, we'd expect the energy to shift to large scales and the *total* enstrophy to more to smaller scales. If the dissipation is non-zero, the total enstrophy will then be dissipated. Bretherton and Haidvogel suggested that the turbulence would thereby act to *minimize* the total enstrophy, while conserving the energy.

To do this, we use the *calculus of variations*, as follows. Let Q be the total enstrophy. Its minimum occurs where its *variation* vanishes. This is as when a function has a maximum or minimum when it's first derivative vanishes. We take the variation thus:

$$\delta Q = \delta \iint \frac{1}{2}(\nabla^2\psi + h)^2 \, dA =$$

$$\iint (\nabla^2\psi + h)\delta(\nabla^2\psi + h) \, dA = 0 \tag{188}$$

We assume the topography is fixed, but the streamfunction can vary. So the equation is:

$$\iint (\nabla^2\psi + h)\delta(\nabla^2\psi) \, dA = 0 \tag{189}$$

Now this could correspond to either a minimum or maximum. To find out, we'd have to evaluate the second variation. We won't do that; we'll simply assume the extremum is a minimum.

However, this only tells us where Q has an extremum. We haven't said anything about the energy. But we can impose energy conservation by using the method of *Lagrange multipliers*. In particular, we define a *functional*:

$$F = Q + \mu(E - E_0) \tag{190}$$

Here the constant μ is a Lagrange multiplier and E is the kinetic energy:

$$E = \frac{1}{2} \iint (u^2 + v^2) \, dA = \frac{1}{2} \iint |\nabla\psi|^2 \, dA \tag{191}$$

E_0 is the kinetic energy of the system (it is a constant).

If we take the variation of F with respect to μ, we get:

$$\frac{\delta F}{\delta \mu} = E - E_0 = 0 \tag{192}$$

So this implies that the solution will have an energy of E_0.

If, on the other hand, we keep μ constant and take the variation of F, we get:

$$\delta F = \delta(Q + \mu(E - E_0)) = \delta Q + \mu \delta E = 0 \tag{193}$$

The variation of E_0 is zero since it is a constant. Substituting in the expressions for Q and E, we have:

$$\delta Q + \mu \delta E = \iint (\nabla^2 \psi + h) \delta(\nabla^2 \psi)\, dA + \mu \iint \nabla \psi \cdot \delta \nabla \psi\, dA \tag{194}$$

Both integrals in (194) can be rewritten using integration by parts, assuming either periodic boundary conditions or that ψ vanishes on the boundaries. So we can write:

$$\iint \nabla \psi \cdot \delta \nabla \psi\, dA = - \iint \nabla^2 \psi \cdot \delta \psi\, dA \tag{195}$$

Also:

$$\iint (\nabla^2 \psi + h) \delta \nabla^2 \psi\, dA = - \iint \nabla (\nabla^2 \psi + h) \cdot \delta \nabla \psi\, dA = \iint \nabla^2 (\nabla^2 \psi + h) \delta \psi\, dA \tag{196}$$

Combining the terms, we get:

$$\delta Q + \mu \delta E = \frac{1}{2} \iint \nabla^2 (\nabla^2 \psi + h - \mu \psi) \delta \psi\, dA = 0 \tag{197}$$

We require that the integral vanish for all variations $\delta \psi$. For this to happen, we must have:

$$\nabla^2\psi + h - \mu\psi = 0 \tag{198}$$

This is is known as the "Euler-Lagrange equation" for the problem. We can solve this by Fourier transforming both the streamfunction and the topography:

$$\psi = \sum_{k,l} \hat{\psi}(k,l) e^{ikx+ily}, \quad h = \sum_{k,l} \hat{h}(k,l) e^{ikx+ily} \tag{199}$$

Substituting both into the Euler-Lagrange equation, we can solve for $\hat{\psi}$ in terms of $\hat{h}$:

$$\hat{\psi} = \frac{\hat{h}}{\mu + k^2 + l^2} = \frac{\hat{h}}{\mu + \kappa^2} \tag{200}$$

Thus the predicted streamfunction resembles the topography. If we know the transform of the topography, we have the transform of the streamfunction. Then we can inverse transform to obtain the actual streamfunction.

But what is this exactly? According to the variational calculation, this is the flow which has the minimum total enstrophy for a given kinetic energy. The minimum enstrophy streamfunction resembles the topography. In other words, the minimum enstrophy solution has flow parallel to the isobaths.

But the flow isn't entire parallel to the isobaths. This is because the denominator in (200) filters the small scales. At large scales, so that $\kappa \ll \mu$, $\psi \approx \hat{h}/\mu$. But at small scales, $\psi \approx \hat{h}/\kappa^2$, which goes to zero as κ gets large. So the flow looks like a low-pass filtered version of the topography. In particular, there will be anticyclonic flow over seamounts and cyclonic flow in basins. This is often observed in the ocean.

What determines μ, the multiplier? If the energy is conserved, then we have:

$$E = \frac{1}{2}\sum_{k,l} \kappa^2 \psi^2 = \frac{1}{2}\sum_{k,l} \frac{\kappa^2 \hat{h}^2}{(\mu + \kappa^2)^2} \tag{201}$$

So if we know the initial energy, we can determine μ. The larger E is, the smaller μ will be. And the smaller μ is, the greater the low-pass filtering effect will be. Thus energetic flows will evolve to more coarse representations of the topography than weak flows.

The results from a numerical simulation from Bretherton and Haidvogel (1976) are shown in Fig. (29). This was a freely-evolving experiment, i.e. one without forcing. The initial streamfunction is shown in the lower left panel and the topography in the upper left panel. After a period of time, the streamfunction settles down into the configuration shown in the lower right panel. The streamfunction strongly resembles the topography, and has the same signs. Thus there is cyclonic flow in the depression in the upper part of the domain. But note too that the streamfunction has less small scale structure than the topography—evidence of the low pass filtering effect predicted by the variational solution.

Observations in the ocean show that mean flows are often correlated with bottom topography. The present theory is one possible explanation for this.

8.4 Stratification

So far, we have looked only at barotropic flows. But the atmosphere and ocean are stratified, and many important dynamics stem from having a stratification. Storms in the atmosphere derive from baroclinic instability,

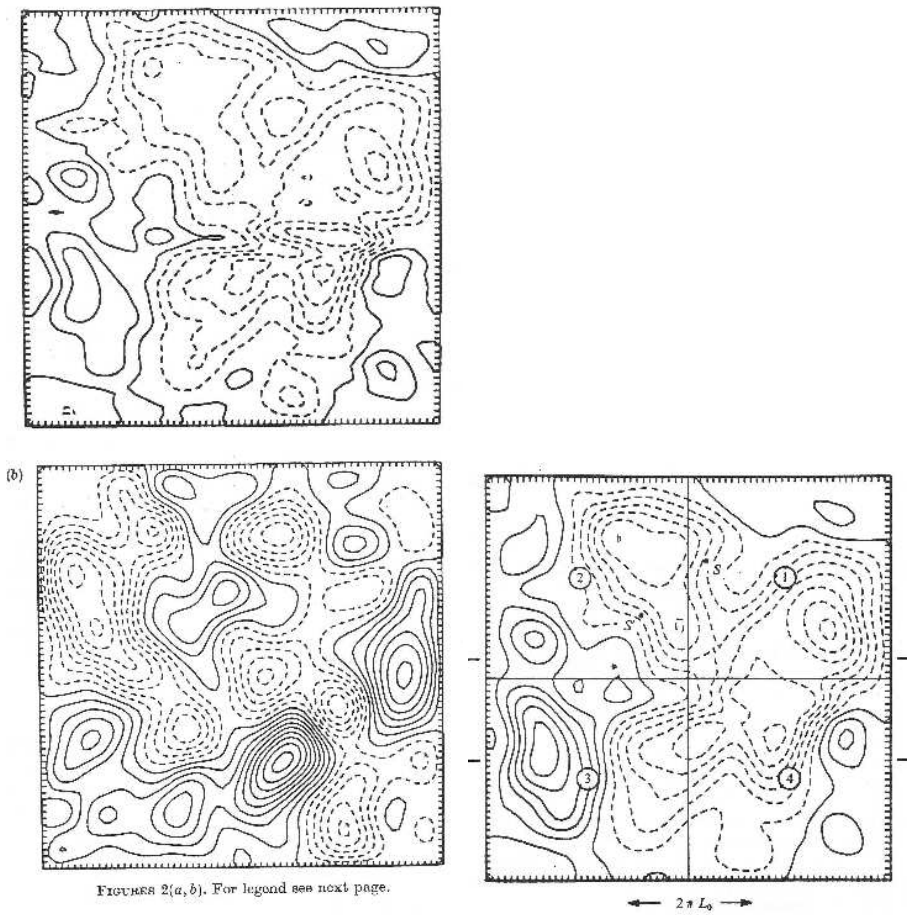

Figure 29: A numerical simulation from Bretherton and Haidvogel (1976). The topography is shown in the upper left panel and the initial streamfunction in the lower left panel. The final streamfunction is shown in the lower right panel. Notice that this is very similar to the topography.

and the Gulf Stream is also known to be thus unstable. In barotropic turbulence, we speak of triad interactions among horizontal wavenumbers. But with stratification, we can furthermore have interactions between waves with different *vertical* structure. Thus the problem becomes three dimensional.

But we are interested in large scale turbulence, and the flow is still predominantly two dimensional at large scales, even with stratification. So it will turn out that many of the concepts we have seen so far will carry over

to the stratified case.

The following will be based on the stratified quasi-geostrophic potential vorticity (QGPV) equation. A derivation is given by Pedlosky (1987) (and is also given in my lecture notes from GEF4500). We will use the Boussinesq form of the QGPV equation. The equation can be written:

$$\frac{\partial}{\partial t}q + \vec{u}_h \cdot \nabla q = 0 \tag{202}$$

where

$$q = \nabla^2\psi + \frac{\partial}{\partial z}(\frac{f_0^2}{N^2}\frac{\partial \psi}{\partial z}) \tag{203}$$

This is the potential vorticity. It is comprised of two parts: the relative vorticity and the *stretching* vorticity. The latter depends on vertical gradients in the streamfunction. N^2 is the Brunt-Vaisala frequency. Note too that the advecting velocities in QG are the horizontal velocities; the vertical velocity is of order Rossby number smaller. Likewise the Laplacian is the horizontal Laplacian, not the three-dimensional one.

For concreteness, we assume we have a periodic domain in (x, y) and solid boundaries at $z = 0$ and $z = 1$. The boundary condition on the vertical boundaries is that the vertical velocity vanishes. This can be shown to be satisfied if $\frac{\partial}{\partial z}\psi = 0$.

8.4.1 Conserved quantities

We can derive an energy equation if we multiply the PV equation by ψ and integrate over the volume:

$$\iiint \psi \frac{\partial}{\partial t}\nabla^2\psi \, dV + \iiint \psi \frac{\partial}{\partial t}\frac{\partial}{\partial z}(\frac{f_0^2}{N^2}\frac{\partial \psi}{\partial z}) \, dV + \iiint \psi \vec{u} \cdot \nabla q \, dV = 0 \tag{204}$$

Note I've dropped the "h" subscript on the velocity. Consider the third term. We can use the following identity:

$$\nabla \cdot (q\vec{u}\psi) = q\psi\nabla \cdot \vec{u} + q\vec{u} \cdot \nabla\psi + \psi u \cdot \nabla q \tag{205}$$

The first term on the RHS is zero from continuity (at first order in the Rossby number). The second term is zero because the velocity is parallel to the streamfunction contours. So the dot product with the gradient is zero. Thus the third term in (204) is:

$$\iiint \psi\vec{u} \cdot \nabla q \, dV = \iiint \nabla \cdot (q\psi\vec{u}) \, dV = \oiint \psi q \, (\vec{u} \cdot \hat{n}) \, dS = 0 \tag{206}$$

after applying Gauss's theorem. This is zero because of periodicity in x and y and because the vertical velocity vanishes at the top and bottom.

Using integration by parts with the first term in (204), we get:

$$\iiint \psi \frac{\partial}{\partial t} \nabla^2 \psi \, dV = -\frac{1}{2} \iiint |\nabla\psi|^2 \, dV = -\frac{1}{2} \iiint (u^2 + v^2) \, dV \tag{207}$$

This is the (horizontal) kinetic energy. Again, only the horizontal velocities contribute to the kinetic energy to a first approximation.

Then there's the other term. Now we apply integration by parts in the vertical:

$$\iiint \psi \frac{\partial}{\partial t} \frac{\partial}{\partial z} \left(\frac{f_0^2}{N^2} \frac{\partial \psi}{\partial z}\right) dV = \iint \psi \frac{\partial}{\partial t} \frac{f_0^2}{N^2} \frac{\partial \psi}{\partial z} \Big|_0^1 \, dA - \frac{1}{2} \frac{\partial}{\partial t} \iiint \frac{f_0^2}{N^2} \left(\frac{\partial \psi}{\partial z}\right)^2 dV \tag{208}$$

The first term on the RHS vanishes because $\frac{\partial}{\partial z}\psi$ vanishes on the vertical boundaries. The second term on the RHS is proportional to the squared temperature; it is the *potential energy*. Thus we have:

$$\frac{\partial}{\partial t}\,\frac{1}{2}\iiint (\frac{\partial \psi}{\partial x})^2 + (\frac{\partial \psi}{\partial y})^2 + \frac{f_0^2}{N^2}(\frac{\partial \psi}{\partial z})^2\, dV = 0 \tag{209}$$

So the total energy—the horizontal kinetic plus potential—is conserved. This is our first conserved quantity.

Now if we multiply the PV equation by q and integrate that over space, we get:

$$\frac{\partial}{\partial t}\frac{1}{2}\iiint q^2\, dV = 0 \tag{210}$$

So the second conserved quantity is the potential enstrophy (the square of the PV).

In fact, there are an infinite number of conserved quantities (see the exercise); but we'll focus on these two.

8.4.2 Energy cascade

With these two conserved quantities, we can demonstrate that the energy shifts to larger scales and the enstrophy to smaller scales, using an argument like Batchelor's (1953), as shown by Charney (1971).

Let's assume that the Brunt-Vaisala frequency, N, is also constant. Then we can redefine the vertical coordinate thus:

$$z^* = \frac{N}{f_0} z \tag{211}$$

Doing this, the PV is simply:

$$q = \nabla^2 \psi + \frac{\partial^2}{\partial z^{*2}} \psi \equiv \nabla_3^2 \psi \tag{212}$$

where ∇_3 is the three dimensional Laplacian, with the new vertical coordinate. Likewise, the energy is:

$$E = \frac{1}{2} \iiint |\nabla_3 \psi|^2 \, dV \tag{213}$$

and the enstrophy is:

$$Q = \frac{1}{2} \iiint (\nabla_3^2 \psi)^2 \, dV \tag{214}$$

We will Fourier transform the streamfunction as follows:

$$\psi(x, y, z) = \sum_{k,l,n} \hat{\psi} e^{ikx+ily} cos(n\pi z) \tag{215}$$

We use the cosine expansion in the vertical so that the vertical derivative of ψ vanishes on the vertical boundaries (at $z = 0$ and $z = 1$). With this, we have:

$$E = \frac{1}{2} \int \kappa^2 |\hat{\psi}|^2 \, d\kappa \tag{216}$$

and

$$Q = \frac{1}{2} \int \kappa^4 |\hat{\psi}|^2 \, d\kappa = \frac{1}{2} \int \kappa^2 E \, d\kappa \tag{217}$$

where

$$\kappa^2 = k^2 + l^2 + n^2 \pi^2 \tag{218}$$

is the total wavenumber squared.

Now we can proceed exactly as in 2-D. Consider a spectrum peaked at some three-dimensional wavenumber, κ_1. We assume the peak will spread, so that:

$$\frac{\partial}{\partial t} \int (\kappa - \kappa_1)^2 E \, d\kappa > 0 \tag{219}$$

Expanding:

$$\frac{\partial}{\partial t}\int \kappa^2 E\, d\kappa - 2\kappa_1 \frac{\partial}{\partial t}\int \kappa E\, d\kappa + \kappa_1^2 \frac{\partial}{\partial t}\int E\, d\kappa > 0 \tag{220}$$

The first and third terms are zero, so;

$$\frac{\partial}{\partial t}\int \kappa E\, d\kappa < 0 \tag{221}$$

which implies the total energy shifts to smaller κ. There is an inverse cascade, as in 2-D turbulence. But note that this is not only to larger horizontal scales—it is also to larger *vertical* scales. This means the flow will become *more barotropic* in time.

8.4.3 The vortex view

Again, we can invoke a vortex view, to obtain a physical impression of this process of barotropization. In geostrophic turbulence, the vortices are *potential vortices*, having both relative and stretching vorticity.

Consider a vortex, with potential vorticity q. We can scale the PV as follows:

$$\begin{gathered} q = \nabla^2\psi + \frac{f_0^2}{N^2}\frac{\partial^2}{\partial z^2}\psi \\ \frac{UL}{L^2} \qquad \frac{f_0^2 UL}{N^2 H^2} \\ 1 \qquad \frac{f_0^2 L^2}{N^2 H^2} \end{gathered} \tag{222}$$

I've divided through by the scaling for the relative vorticity, and I'm taking N^2=const. We see that the relative scale of the stretching vorticity depends on the vortex size, L. We can rewrite this term as:

$$\frac{f_0^2 L^2}{N^2 H^2} = \frac{L^2}{L_d^2} \tag{223}$$

where

$$L_d = \frac{NH}{f_0} \tag{224}$$

is the *deformation radius*. If the vortex is much larger than the deformation radius, the stretching vorticity dominates and if the vortex is much smaller than L_d, the relative vorticity dominates.

Imagine we have a three-dimensional QG simulation, with random initial flow. The flow will organize itself into vortices, on different *levels* in the flow. These vortices will be smaller than the deformation radius and dominated by relative vorticity. So they will behave just like vortices in 2-D turbulence. Like-sign vortices will merge, making larger vortices.

As the vortices become larger, the stretching vorticity is more important. We see, in particular, that the vortices have greater vertical extent. So they begin to interact with vortices on other levels. Occasionally, like-sign vortices will vertically *align* with one another. This is just like a merger, but between two vortices on different levels.

The flow thus evolves to a system of fewer and fewer vortices, with greater and greater vertical extent. This is the physical meaning of Charney's 3-D cascade.

The potential vorticity from such a simulation, from McWilliams et al. (1999), is shown in Fig. (30). The flow started with a 3-D random initial condition. In the upper panel is the PV at an intermediate time. Already it is clear that like-sign vortices are congregating together. At a later time, shown in the lower panel, the vertical alignment is clear, and two large tornado-like structures have formed.

Thus the vortex view again illustrates the behavior that we have deduced from spectral considerations.

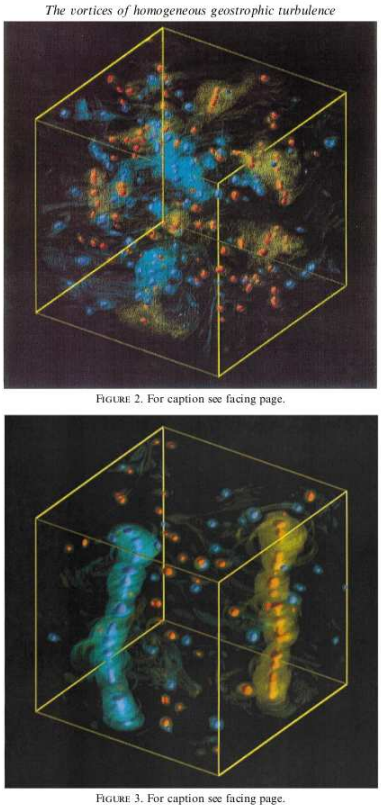

Figure 30: Potential vorticity from a 3-D QG simulation from random initial conditions. The upper panel shows the PV at an intermediate time and the lower panel at a late time. Note the vertical alignment of the vortex structures.

8.4.4 Enstrophy cascade

Another prediction of Charney's is that there will be an enstrophy cascade in quasi-geostrophic turbulence. This will have an energy spectrum given by:

$$E(\kappa) \propto \eta^{-2/3}\kappa^{-3} \tag{225}$$

where η is now the total enstrophy transfer rate, with units of sec^{-3}. The difference here is that the wavenumber is the full three-dimensional wavenumber given above. However, Charney assumes that the turbulence is *iso-*

tropic in the three directions, (x, y, z^*). That implies that the energy spectrum will be the same for the horizontal kinetic energy, or indeed even one component, i.e. for u^2.

This is a possible explanation for the κ^{-3} range below 2000 km in the Nastrom and Gage spectra in Fig. (22). The atmosphere is not a 2-D fluid, but at large scales it is quasi-geostrophic. Moreover, in the troposphere the Brunt-Vaisala frequency is approximately constant, so Charney's stretched vertical coordinate is a reasonable choice. Further analysis has shown that the enstrophy flux in this range is downscale, as expected for an enstrophy cascade (Lindborg, 1999). So it seems like this really is an enstrophy cascade.

There are *also* indications of an enstrophy cascade in the ocean. Wang et al. (2009) calculated energy spectra from current measurements collected from a ferry steaming between the U.S. and Bermuda, across the Gulf Stream. The results (Fig. 31) also show a clear κ^{-3} range. The peak of the scale corresponds to roughly the 50 km scale. In addition, the kinetic and potential energy show the same slope, consistent with Charney's assumption of an energy flow which is isotropic in the three dimensional wavenumber.

Thus the addition of stratification hasn't changed the situation greatly. However, as the flow becomes more barotropic, the boundaries will eventually become important. So it may be that Charney's construction works better at small scales, i.e. in the enstrophy range. Moreover, where does baroclinic instability fit in? Instability implies a conversion of large scale potential energy to kinetic energy at the deformation radius. How do we reconcile this with an inverse cascade? The answer can be found in detailed consideration of the triad interactions occurring in a baroclinic sys-

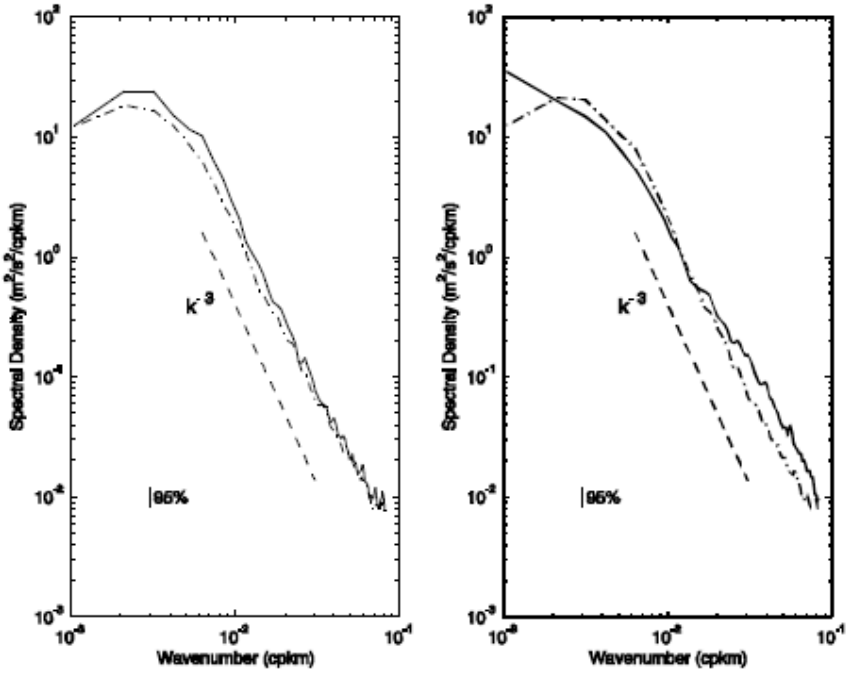

Figure 31: Kinetic energy spectra from ADCP data collected from a ferry steaming between the U.S. and Bermuda. The left panel shows the u and v components, and the right panel the kinetic and potential energies. From Wang, Flagg, Donohue and Rossby (2009).

tem (next section).

Exercise: *Enstrophy conservation*

Show that *any* function of the potential vorticity q is also conserved in the QG system.

8.4.5 Cascades in a two mode system

Triad interactions become very complicated when we have vertical modes in addition to the horizontal wavenumbers. However, we can get a good idea of how the system behaves when we consider only two vertical modes.[11]

Consider again the PV equation, which we write thus:

[11] The following is based on Salmon (1980).

$$\frac{\partial}{\partial t}q + u\frac{\partial}{\partial x}q + v\frac{\partial}{\partial y}q = \frac{\partial}{\partial t}q - \frac{\partial \psi}{\partial y}\frac{\partial}{\partial x}q + \frac{\partial \psi}{\partial x}\frac{\partial}{\partial y}q = 0 \tag{226}$$

We can write this in shorthand form thus:

$$\frac{\partial}{\partial t}q + J(\psi, q) = 0 \tag{227}$$

The $J(,)$ function is called the *Jacobian*. It is defined as:

$$J(a, b) = \frac{\partial a}{\partial x}\frac{\partial b}{\partial y} - \frac{\partial b}{\partial x}\frac{\partial a}{\partial y} \tag{228}$$

We'll take $N = const.$, so the PV is:

$$q = \nabla^2 \psi + \frac{f_0^2}{N^2}\frac{\partial^2}{\partial z^2}\psi \tag{229}$$

Assuming the fluid depth is such that $0 \leq z \leq H$, we can express the streamfunction in terms of *vertical modes*, thus:

$$\psi(x, y, z, t) = \sum_n \psi_n(x, y, t) cos(\frac{n\pi z}{H}) \tag{230}$$

We will only consider the first two terms:

$$\psi(x, y, z, t) = \psi_B(x, y, t) + \psi_T(x, y, t)\, cos(\frac{n\pi z}{H}) \tag{231}$$

Here ψ_B is the *barotropic* streamfunction; it does not vary in the vertical. ψ_T is the ***first baroclinic*** mode. It is the gravest of the cosine modes; if we integrate it in the vertical, it vanishes. We will exploit this below.

The PV also has two components:

$$q = \nabla^2 \psi_B + (\nabla^2 - F)\psi_T\, cos(\frac{n\pi z}{H}) \tag{232}$$

where

$$F = \frac{\pi^2 f_0^2}{N^2 H^2} \tag{233}$$

Notice that this parameter has units of L^{-2}. Thus the square root of F is like a wavenumber. This corresponds to the inverse of the deformation radius.

Plugging the streamfunction and PV into the PV equation, we get:

$$\frac{\partial}{\partial t}\nabla^2\psi_B + \frac{\partial}{\partial t}(\nabla^2 - F)\psi_T cos(\frac{n\pi z}{H}) + J(\psi_B, \nabla^2\psi_B) +$$
$$J(\psi_B, (\nabla^2 - F)\psi_T)cos(\frac{n\pi z}{H}) + J(\psi_T, \nabla^2\psi_B)cos(\frac{n\pi z}{H}) +$$
$$J(\psi_T, (\nabla^2 - F)\psi_T)cos^2(\frac{n\pi z}{H}) = 0 \tag{234}$$

We can isolate the time derivative of the barotropic streamfunction if we integrate this equation in z over the depth of the fluid, and then divide by the depth H:

$$\frac{\partial}{\partial t}\nabla^2\psi_B + J(\psi_B, \nabla^2\psi_B) + \frac{1}{2}J(\psi_T, (\nabla^2 - F)\psi_T) = 0 \tag{235}$$

The terms multiplied by cosine vanish, and the cosine squared term integrates to one half. This is the vorticity equation for the barotropic mode. Notice that the barotropic vorticity can change by two terms. The first involves the barotropic velocity advecting the barotropic vorticity, and the second the baroclinic velocity advecting the baroclinic vorticity.

Similarly, we can obtain an equation for the baroclinic vorticity if we multiply the equation by $cos(n\pi z/H)$ and integrate over the depth. Then we get:

$$\frac{\partial}{\partial t}(\nabla^2 - F)\psi_T + J(\psi_B, (\nabla^2 - F)\psi_T) + J(\psi_T, \nabla^2\psi_B) = 0 \qquad (236)$$

after cancelling a common factor of 1/2. This is the baroclinic vorticity equation. This states the baroclinic PV changes when the barotropic velocity advects baroclinic PV, and vice versa.

Each PV equation has an energy relation associated with it. If we multiply (235) by ψ_B and integrate over the area of the domain, we get:

$$\frac{d}{dt}\iint |\nabla\psi_B|^2 \, dA - \iint \psi_B J(\psi_T, (\nabla^2 - F)\psi_T) \, dA = 0 \qquad (237)$$

after integrating by parts. Note the barotropic advection term vanishes when integrated over the area. The first term is the barotropic energy, which is purely kinetic. This is *not* conserved, because of the interaction with the baroclinic mode.

Likewise, multiplying (236) by ψ_T and integrating over area, we get:

$$\frac{d}{dt}\iint [|\nabla\psi_T|^2 + F|\psi_T|^2] \, dA - \iint \psi_T J(\psi_B, (\nabla^2 - F)\psi_T) \, dA = 0 \quad (238)$$

again, after integration by parts. The first term is the change in the total baroclinic energy, which has both kinetic and potential parts. The baroclinic energy isn't conserved either, due to the interaction with the barotropic mode.

However, if we integrate by parts again, we can show that:

$$-\iint \psi_B J(\psi_T, (\nabla^2 - F)\psi_T) \, dA = \iint \psi_T J(\psi_B, (\nabla^2 - F)\psi_T) \, dA \quad (239)$$

So adding the two equation energy equations together, we get:

$$\frac{d}{dt}\iint |\nabla\psi_B|^2 + |\nabla\psi_T|^2 + F|\psi_T|^2\, dA = 0 \tag{240}$$

So the total energy, barotropic plus baroclinic, is conserved.

After a similar derivation, you can show that:

$$\frac{d}{dt}\iint (\nabla^2\psi_B)^2 + ((\nabla^2 + F)\psi_T)^2\, dA = 0 \tag{241}$$

So the total enstrophy is also conserved.

Now, how energy is transferred in the two mode system depends on the triad interactions. To see how these work, we'll focus on the barotropic PV equation (235). We write this for Fourier components, and we leave out the summations for simplicity. The equation then looks like this:

$$-\frac{\partial}{\partial t}(k_x^2 + k_y^2)\psi_{B1}e^{ik\cdot x} + J(\psi_{B2}, -(m_x^2 + m_y^2)\psi_{B3})e^{im\cdot x + in\cdot x}$$
$$+J(\psi_{T1}, -(q_x^2 + q_y^2 + F)\psi_{T2})e^{ip\cdot x + iq\cdot x} = 0 \tag{242}$$

Note that I'm using n now as a horizontal wavenumber (not the vertical mode number). To extract an equation for the barotropic streamfunction with wavenumbers (k_x, k_y), we multiply by $\psi_{B1}e^{-ik\cdot x}$ and integrate over the area. The result is:

$$-\frac{\partial}{\partial t}(k_x^2 + k_y^2)|\psi_{B1}|^2 + Re\{\psi_{B1}^* J(\psi_{B2}, -(m_x^2 + m_y^2)\psi_{B3})\}\delta(m + n - k)$$
$$+Re\{\psi_{B1}^* J(\psi_{T1}, -(q_x^2 + q_y^2 + F)\psi_{T2})\}\delta(p + q - k) = 0 \tag{243}$$

This equation accounts for the change in barotropic energy at wavenumber (k_x, k_y). Remember that the two advection terms involve sums over many wavenumbers. Interactions between wavenumber triads can transfer energy.

We see though that there are two types of triad. The first involves interactions between three barotropic waves. This corresponds to the triads we considered previously. The second though is something new, and involves the barotropic wave (at (k_X, k_y)) and two baroclinic waves.

Consider a triad of barotropic waves first. These conserve barotropic energy and enstrophy:

$$\frac{d}{dt}(E_1 + E_2 + E_3) = 0$$
$$\frac{d}{dt}(Z_1 + Z_2 + Z_3) = 0 \tag{244}$$

We can rewrite the enstrophy relation thus:

$$\frac{d}{dt}(\kappa_1^2 E_1 + \kappa_2^2 E_2 + \kappa_3^2 E_3) = 0 \tag{245}$$

This is exactly like Fjørtoft's barotropic example. We expect then that energy will shift to larger scales and enstrophy to smaller scales.

Now consider the barotropic/baroclinic triads. The enstrophy relations are:

$$\frac{d}{dt}(\kappa_1^2 E_1 + (\kappa_2^2 + F) E_2 + (\kappa_3^2 + F) E_3) = 0 \tag{246}$$

This is more complicated than the barotropic case because of the F terms (which also affect the baroclinic energies). Consider first that all three members of the triad have scales well below the deformation radius, so that $(\kappa_1, \kappa_2, \kappa_3) \gg F$. Then the enstrophy equation is, approximately:

$$\frac{d}{dt}(\kappa_1^2 E_1 + \kappa_2^2 E_2 + \kappa_3^2 E_3) = 0 \tag{247}$$

This is the same as with the barotropic triad. Thus we expect energy to be transferred to the triad member with the largest scale (regardless of

whether this is barotropic or baroclinic). Energy would thus shift toward the deformation radius.

Now consider that we have a large scale triad, so that $(\kappa_1, \kappa_2, \kappa_3) \ll F$. Then we have, approximately:

$$\frac{d}{dt}(FE_2 + FE_3) = 0 \tag{248}$$

This simply states that energy will pass between the two baroclinic waves. But the direction of transfer is undetermined—we can't say whether energy is moving up or downscale.

Does this mean that baroclinic energy at large scales can't transition to smaller scales? It would seem so. But what about baroclinic instability? In that, energy is transferred from a baroclinic mean shear to barotropic eddies. This would seem to contradict the present finding. In fact the problem here is the assumption of *local* interactions. What about a non-local interaction, between a large scale baroclinic mode and smaller scale barotropic and baroclinic waves?

The usual models of baroclinic instability (the Eady model, the Charney model and the Philips model) all involve a baroclinic shear with no lateral shear. So we could express this as a baroclinic mode in which:

$$(\kappa_2^2 + F)\psi_{T1} = F\psi_{T1} \tag{249}$$

(the Laplacian is zero because the mode is constant in x and y). Making no other assumptions about scales, we have:

$$\frac{d}{dt}(E_1 + E_2 + E_3) = 0$$

$$\frac{d}{dt}(\kappa_1^2 E_1 + FE_2 + (\kappa_3^2 + F)E_3) = 0 \tag{250}$$

Using the first equation, we can eliminate dE_2/dt from the enstrophy equation. This yields:

$$\frac{d}{dt}(\kappa_1^2 E_1 - F E_1 - F E_3 + (\kappa_3^2 + F) E_3) = 0 \tag{251}$$

or:

$$\frac{d}{dt}\kappa_3^2 E_3 = \frac{d}{dt}((F - \kappa_1^2) E_1) \tag{252}$$

This implies that the energy in both the other modes can increase in time if:

$$\kappa_1^2 < F \tag{253}$$

In other words, if the barotropic wave is larger than the deformation radius, it can take energy from the primary baroclinic wave. This is precisely the short-wave cut-off that we found when we studied the Eady model—only the long waves can be unstable.

But more than that, the barotropic wave can be much smaller than the primary baroclinic wave. Recall that the most unstable wave in the Eady problem has a scale somewhat larger than the deformation radius. Such a triad is *non-local*, because there is a large separation in scales between the triad members.

We can summarize the results by using a schematic diagram (Fig. 32), which is based on Salmon's (1980). The energy at small scales cascades to larger scales in both the baroclinic and barotropic modes via local interactions. Baroclinic modes with scales larger than the deformation radius are unstable and transfer energy non-locally to the barotropic modes. Then energy eventually cascades locally to large scales in the barotropic mode.

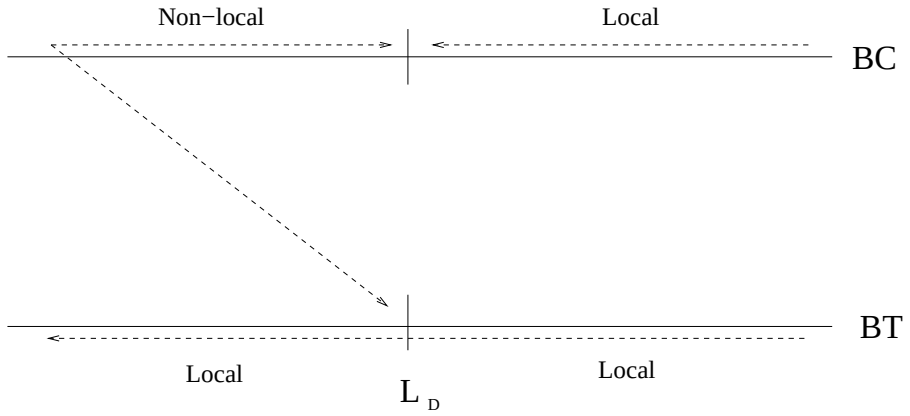

Figure 32: A idealized diagram indicating the tendencies for energetic transfer in the two layer model. The upper line represents the baroclinic mode and the lower line the barotropic mode. Based on a figure of Salmon's (1980).

An important point here is that baroclinic instability in this turbulence context is simply a non-local triad interaction. This means that the transfer to the barotropic mode is *generic* for large scale baroclinic modes. Thus, for example, a large scale baroclinic Rossby wave can be unstable too (LaCasce and Pedlosky, 2004; Isachsen et al., 2008). There is no need to have a stationary flow, as employed in the Eady, Charney and Philips models.

9 Turbulent Diffusion

Now we will focus on how turbulent flows advect passive tracers, and in particular what happens with particles and pairs of particles. In section (7.6), we examined how the spectrum of passive tracer variance would look in a given turbulent inertial range. In that case, we treated the tracer as a continuous Eulerian field, like vorticity. But now we will take a more Lagrangian view.

9.1 Single particle dispersion

9.1.1 Random walk

The essence of single particle motion is captured in the *random walk* or "drunkard's walk" problem. This is the basis of "Brownian motion", as studied by Einstein (1905). Consider an idealized drunk person. Imagine he takes uniform steps, of length s. But because he is drunk, each step is randomly oriented and uncorrelated with the previous step. We can write his position as:

$$\vec{D}_n = \vec{D}_{n-1} + \vec{s} \tag{254}$$

where $\vec{s}$ is the random displacement. So the squared displacement of the drunk is:

$$|\vec{D}_n|^2 = |\vec{D}_{n-1}|^2 + s^2 + \vec{D}_{n-1} \cdot \vec{s} \tag{255}$$

where s is the magnitude of $\vec{s}$. Now, if we have a party of drunks, each moving in this way, we can average the mean square displacement for the whole group. If you think of a "cloud" of drunks, the root mean square displacement is proportional to the cloud's radius. Averaging, we get:

$$< |\vec{D}_n|^2 >=< |\vec{D}_{n-1}|^2 > +s^2 \tag{256}$$

where the brackets indicate an average over all the drunks. The cross correlation term vanishes because the drunks' steps are uncorrelated with their previous steps. Now, assuming the drunks all start at the pub, at zero displacement, we have:

$$< |\vec{D}_1|^2 >= 0 + s^2 \tag{257}$$

and

$$< |\vec{D}_2|^2 >= 2s^2 \tag{258}$$

so

$$< |\vec{D}_n|^2 >= ns^2 \tag{259}$$

Thus the root mean square displacement is:

$$(< |\vec{D}_n|^2 >)^{1/2} = \sqrt{n}s \tag{260}$$

If the drunks take steps at uniform time, e.g. one step per second, then the rms displacement grows as $t^{1/2}$ power. This is a characteristic feature of Brownian motion. We will see later that single particle dispersion behaves the same way, when the particle motion is uncorrelated.

9.1.2 Diffusion

Now we will show that a diffusing cloud, with a constant diffusivity, has a radius which also increases as $t^{1/2}$ power. The equation for a passive tracer was given in (127). Now we will consider what happens to the tracer in the absence of advection, so that the equation is:

$$\frac{\partial}{\partial t}C = \kappa \nabla^2 C \tag{261}$$

We define the variance of the cloud as:

$$< r^2 >= \frac{\iint r^2 C \, dA}{\iint C \, dA} \tag{262}$$

The variance is essentially the radius squared of the cloud of tracer. We are interested in how this changes in time, i.e. $\frac{\partial}{\partial t} < r^2 >$. We can obtain an

equation for this by multiplying the tracer equation by r^2 and integrating over space. Assuming that the spreading is isotropic (the same in every direction), we have (using cylindrical coordinates):

$$\frac{\partial}{\partial t}\int_0^\infty r^2 C\, r dr = \int_0^\infty r^2\, \kappa\, \frac{1}{r}\frac{\partial}{\partial r}(r\frac{\partial}{\partial r}C)\, r dr$$

$$= -2\kappa \int_0^\infty r^2 \frac{\partial}{\partial r} C\, dr = 4\kappa \int_0^\infty C\, r dr \tag{263}$$

after using integration by parts. Thus:

$$\frac{\partial}{\partial t} < r^2 >= \frac{\partial}{\partial t}\frac{\iint r^2 C\, dA}{\iint C\, dA} = 4\kappa \tag{264}$$

Integrating this in time, we get:

$$< r^2 >= 4\kappa t \tag{265}$$

So the rms radius of the cloud increases as $t^{1/2}$, just as in a random walk. So a random walk is a *diffusive process*. Drunks drifting from a pub behave as a passive tracer, diffusing with a constant diffusivity. We often call the time rate of change of the variance the "diffusivity" when dealing with particles.

An alternate way of deriving the same result is to use the exact solution to (261). Assume that the initial tracer distribution is a delta function at the origin (as if all the the drunks are initially at a pub at $r = 0$). One can show that the solution to (261) is given by:

$$C = \frac{1}{2\pi\kappa t} exp(-\frac{r^2}{4\kappa t}) \tag{266}$$

The prefactor guarantees that:

$$\int_0^\infty C\, r\, dr = 1 \tag{267}$$

We can use this solution to find the variance of the cloud. The result is:

$$< r^2 >= 4\kappa t \tag{268}$$

9.1.3 Single particle dispersion

We've seen that randomly walking particles are essentially diffusing in space. Taylor (1921) formalized this, in the following way.

Imagine we have a collection of particles. We can define the diffusivity (in the x-direction) of the particle cloud by:

$$K \equiv \frac{1}{2}\frac{d}{dt} < X^2 >=< u(t)X(t) > \tag{269}$$

The factor of $1/2$ is traditional, and cancels the other two when taking the derivative. Realizing that the displacement at time t is just the integral of the velocity, we can rewrite this as:

$$K =< u(t) \int_0^t u(t')dt' >= \int_0^t < u(t)\, u(t') > \, dt' \tag{270}$$

Now if the velocity field is *stationary* (not changing in time), we can write:

$$K = \nu^2 \int_0^t R(t') \, dt' \tag{271}$$

where

$$R(t) \equiv \frac{1}{\nu^2} < u(0)\, u(t') > \tag{272}$$

and where ν^2 is the velocity variance for the particles. Note that we can substitute $u(0)$ for $u(t)$ because of stationarity (the velocity on average is the same at any time).

The function $R(t)$ is the normalized integral of the velocity *autocorrelation*. For the random walk, the velocity is uncorrelated at each step. But generally the velocity is correlated for some period.

Taylor (1921) noticed that the diffusivity should behave the same in the limits of short and long times. At short times, the autocorrelation can be expanded in a Taylor series:

$$R(t) = 1 + \frac{dR}{dt}t + ... \tag{273}$$

As $t \rightarrow 0$ then, $R \rightarrow 1$ (the limit is one because we normalized by the velocity variance, ν^2). Thus we have:

$$lim_{t\rightarrow 0}\ K = \nu^2 t \tag{274}$$

Thus the dispersion, $< X^2 >$, increases as t^2.

At long times, the behavior is also similar for diverse flows. Assuming that the velocity eventually becomes decorrelated, we expect the integral of the autocorrelation to converge:

$$T_L = \frac{1}{\nu^2}\int_0^\infty R(t')dt' = const. \tag{275}$$

The integral has units of time and is known as the *Lagrangian integral time*. T_L gives an indication of the predictability of the particle motion, i.e. how long the velocity is correlated with itself. Thus the diffusivity is:

$$lim_{t\rightarrow\infty}\ K = \nu^2 T_L \tag{276}$$

and this is constant. We say that the system is *diffusive*, and hence can be modeled using a diffusion-type equation. Furthermore, the dispersion will

increase as t, exactly as the mean square radius increases under a random walk.

Thus an implication of Taylor's work is that we can represent many particle dispersion problems as a random walk. We can, for instance, model ash spreading from a volcano as a mixture of advection (left out here, but important) and a random walk. This opens the possibility for *stochastic models* for pollution spreading.

But there is a downside as well. Since single particle motion has such generic limits, it is not so useful when one is trying to distinguish different types of flow. Say for example you would like to know whether there is an energy or enstrophy cascade occurring. In both cases, the single particle diffusivity should asymptote to a constant. We return to this shortly.

9.1.4 The vortex merger problem

In section (7.5), we showed that freely evolving 2-D turbulence can be viewed as a merger process between discrete vortices. Carnevale et al. (1991) constructed a theory in which the important flow statistics, like the enstrophy, could be deduced from the vortex population. The only unknown in their theory was the decay rate of the vortex density, ρ. Here we show that can be accounted in terms of the dispersion of the vortices.[12].

The numerical experiment in this case was a freely-evolving, 2-D turbulence simulation in a periodic domain, from random initial conditions. Vortices emerge at the early times and begin merging. At some point, particles were deployed in the flow, and the dispersion of the particles and vortices was compared (left panel of Fig. 33). We see that after a short time, the dispersion for vortices and particles is statistically indistinguish-

[12]The section follows LaCasce (2008)

able. That implies that the vortices are dispersing exactly like the passive particles. Note too that the dispersion is increasing *faster* that diffusively. A best fit of the data suggests:

$$< X^2 > \propto t^{1.3} \tag{277}$$

This implies that the diffusivity increases as $t^{0.3}$. Such dispersion is called "super-diffusive", since the spreading is greater than in a random walk.

As the vortex dispersion matches the particles', we can think of a diffusivity to characterize the vortex spreading. We can scale the diffusivity thus:

$$D = \frac{1}{2}\frac{d}{dt} < X^2 > = < uX > \propto UL \tag{278}$$

where U is the mean vortex velocity and L is the typical spacing between vortices. Now if we have a vortex density of ρ, then the typical spacing is:

$$L \propto \rho^{-1/2} \tag{279}$$

The velocity on the other hand scales as the square root of the total energy, given in (119):

$$U \propto E^{1/2} \propto \rho^{1/2} \zeta_c \, b^2 \tag{280}$$

So the diffusivity scales as:

$$D \propto UL \propto \rho^{1/2} \zeta_c \, b^2 \rho^{-1/2} \propto \Gamma \tag{281}$$

where

$$\Gamma = \zeta_c \, \pi b^2 \tag{282}$$

is the mean vortex *circulation*. So the diffusivity and the circulation should behave the same way. In the experiment shown in the left panel of Fig. (**??**), the diffusivity scales as:

$$D = \frac{1}{2}\frac{d}{dt} < X^2 > \propto t^{0.3} \tag{283}$$

So the circulation, if this argument is correct, should scale the same way.

Shown in the right panel of Fig. (33) are the exponents, α, obtained from a suite of experiments with different initial conditions and different types of small scale damping. We see that the exponents tend to be between 0.2-0.4, for both the diffusivity and circulation, for most of the experiments. The average value for the exponent is roughly $\alpha = 1/3$.

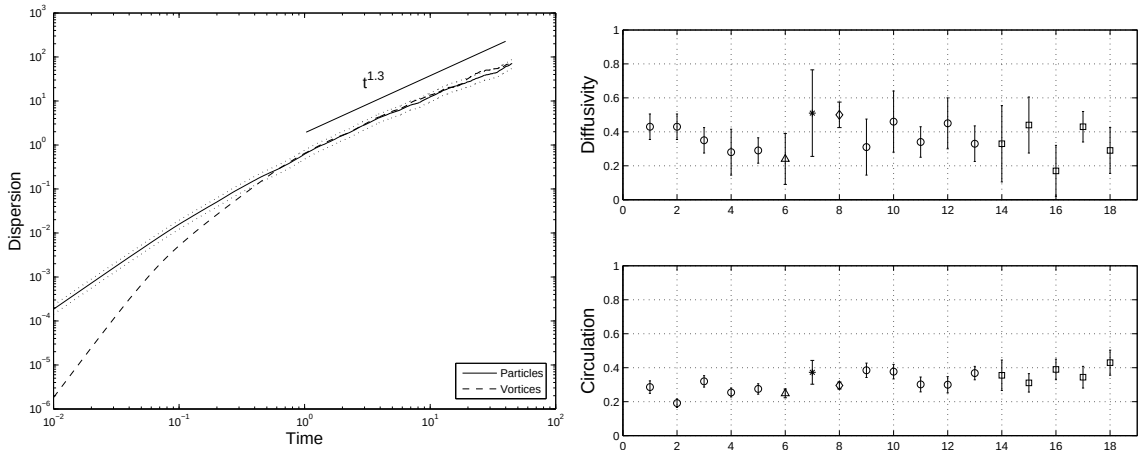

Figure 33: The dispersion for vortices (solid curve) and passive particles (dashed line) in a 2-D turbulence simulation (left panel). Shown in the right panel are the growth exponents, α, from various runs for the vortex diffusivity and the mean vortex circulation. The value is usually between 0.2-0.4. From LaCasce (2008).

If we know the scaling for the circulation, we can find the decay rate for the density. This is because the total energy is conserved. So:

$$E = \rho\zeta_c^2 b^4 = \rho\Gamma^2 = const. \tag{284}$$

Thus:

$$\rho \propto \Gamma^{-2} \propto t^{-2/3} \tag{285}$$

This is close to the value, 0.7, inferred by McWilliams (1990) and Weiss and McWilliams (1993) (sec. 7.5). In other simulations, we find a value of $2/3$ (Fig. 34), using a range of different initial conditions.

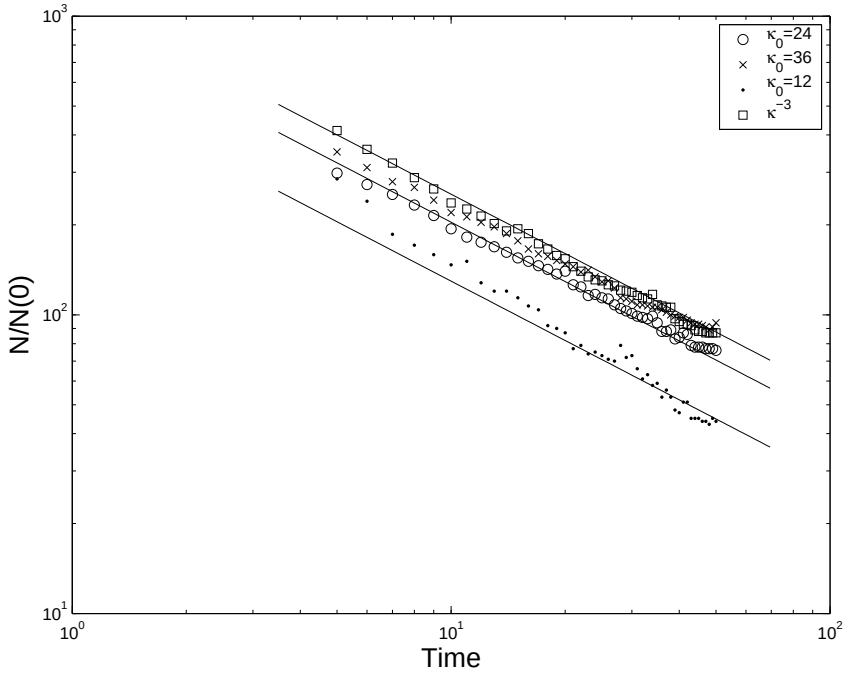

Figure 34: Vortex density from 4 experiments with different initial conditions. The lines indicate a decay of $t^{-2/3}$. From LaCasce (2008).

The results shown in Fig. (33) are from numerical experiments with very weak lateral damping. Increasing the damping accelerates the vortex decay, because lateral diffusion causes the vortices to spread out, hence increasing their chance for collisions. But nevertheless, it is fruitful to think of vortex merger as a dispersion problem.

Note though that this problem has not been completely solved! All

we've done is to shift the unknown. Previously, we didn't know what set the density decay. Now we know that, but we don't know what determines the dispersion exponent. So there is still work to be done.

9.2 Two particle dispersion

As noted, the single particle dispersion exhibits generic behavior and so is not terribly useful for differentiating different types of flow. Better in this regard is the dispersion between *two* particles, called "relative dispersion". Rather than study how a particle drifts from its starting location, we see how two particles separate in time. An advantage is that two particle dispersion is unaffected by a constant background flow, U, whereas single particle dispersion is.

Two particle dispersion is:

$$< |\vec{x}_1(t) - \vec{x}_2(t)|^2 > = < |\vec{x}_1(t)|^2 > + < |\vec{x}_2(t)|^2 > - 2 < \vec{x}_1 \cdot \vec{x}_2 > \quad (286)$$

If the flow is *homogeneous*, then:

$$< |\vec{x}_1(t)|^2 > = < |\vec{x}_2(t)|^2 > = < x^2(t) > \quad (287)$$

where $< x^2(t)$ is the single particle dispersion. Thus:

$$< |\vec{x}_1 - \vec{x}_2|^2 > = 2 < x^2 > - 2 < \vec{x}_1 \cdot \vec{x}_2 > \quad (288)$$

Now if the two particles are moving independently of one another, i.e. if their velocities are uncorrelated, the cross correlation term will be zero. This is what typically happens when the particles are far apart. Then two particle dispersion is like single particle dispersion. If we define the two particle diffusivity, then in this limit we have:

$$K_2 \equiv \frac{1}{2}\frac{d}{dt} < |\vec{x}_1 - \vec{x}_2|^2 >= 2K_1 \tag{289}$$

where K_1 is the single particle diffusivity.

But what happens when the particle motion *is* correlated? This is where relative dispersion is interesting. Two particles are measuring the velocities at the points in space and time where the particles are (Fig. 35). Thus the difference between the particle velocities is equal to the difference in Eulerian velocities at that time and location. Now if the flow is homogeneous, the mean square velocity difference for particles with a separation r is the same as the mean square velocity difference for any two points in the flow also with a separation r. This velocity difference is sometimes called the "second order structure function".

In turbulence, this scales with energy or enstrophy transfer rate, just as the spectrum does. So in the energy cascade, we have:

$$< |\vec{u}_1 - \vec{u}_2|^2 > \propto \epsilon r^{2/3} \tag{290}$$

The two thirds can be deduced from dimensional grounds: ϵ has units of m^2/sec^3 and the square velocity difference has units of m^2/sec^2. This relation is known as "Kolmogorov's 2/3 Law".

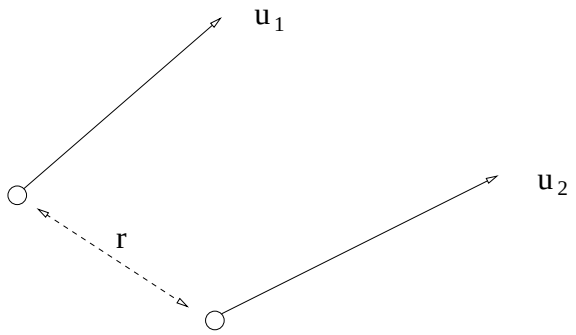

Figure 35: Two particles moving in a flow.

In the enstrophy range, we find:

$$< |\vec{u}_1 - \vec{u}_2|^2 > \propto \eta r^2 \tag{291}$$

So the velocity difference increases more rapidly with separation in the enstrophy range.

We can deduce corresponding relations for the relative diffusivity. In the energy range, the diffusivity scales as:

$$K_2 \propto \epsilon^{1/3} r^{4/3} \tag{292}$$

because the diffusivity has units of m^2/sec. This relation was first noticed by Richardson (1926). The connection to Kolmogorov's theory was made by Obukhov (1941) and Batchelor (1952). Notice that this implies:

$$\frac{d}{dt} < (x_1 - x_2)^2 > = \frac{d}{dt} < r^2 > \propto \epsilon^{1/3} r^{4/3} \tag{293}$$

If we integrate this, we find that:

$$< r^2 > \propto \epsilon t^3 \tag{294}$$

Integrating (293) is not strictly correct, because the LHS involves the mean square separation, not the separation. But from a scaling perspective, this is reasonable. The cubic growth is now known as "Richardson's Law".

In the enstrophy range, dimensional arguments suggest:

$$\frac{d}{dt} < r^2 > \propto \eta^{1/3} r^2 \tag{295}$$

Integrating this in time, we get:

$$< r^2 > \propto exp(\eta^{1/3} t) \tag{296}$$

This is sometimes called "Lin's Law", after Lin (1972). So separations in the enstrophy range grow exponentially in time.

These results can be compared with those that we derived for predictability, in sec. (7.7). In the enstrophy range, the scale of the error was found to increase as $exp(\eta^{1/3}t)$—exactly as the separation in particles increases here. Similarly, in the energy range we found:

$$T = \int_{\kappa 0}^{\kappa 1} \epsilon^{-1/3}\kappa^{-5/3}\, d\kappa \approx \epsilon^{-1/3}\kappa^{-2/3}|_{\kappa 0}^{\kappa 1} \approx \epsilon^{-1/3}\kappa_0^{-2/3} \tag{297}$$

This implies that the length scale scales as:

$$L_0^{2/3} \propto \epsilon^{1/3}T \tag{298}$$

as $L_0 = 2\pi/\kappa_0$. Thus:

$$L_0^2 \propto \epsilon T^3 \tag{299}$$

The predictability relations are thus identical in form to the two particle dispersion relations. This is not coincidental. In fact, two particle dispersion is actually a measure of Lagrangian predictability. If we change the initial condition of a particle slightly, the growth of the error is determined by relative dispersion.

How do these predictions compare to observations? Morel and Larcheveque (1974) calculated pair statistics for pairs of balloons deployed in the lower stratosphere in the Southern Hemisphere during the French EOLE experiment. The dispersion is seen to grow exponentially in time, during the first 6 days and up to scales of 1000-2000 km. Thereafter, the two particle dispersion increases linearly in time. From the turbulence perspective, we

would interpret this as evidence of an enstrophy cascade at scales below 1000 km, and random, uncorrelated motion at larger scales.

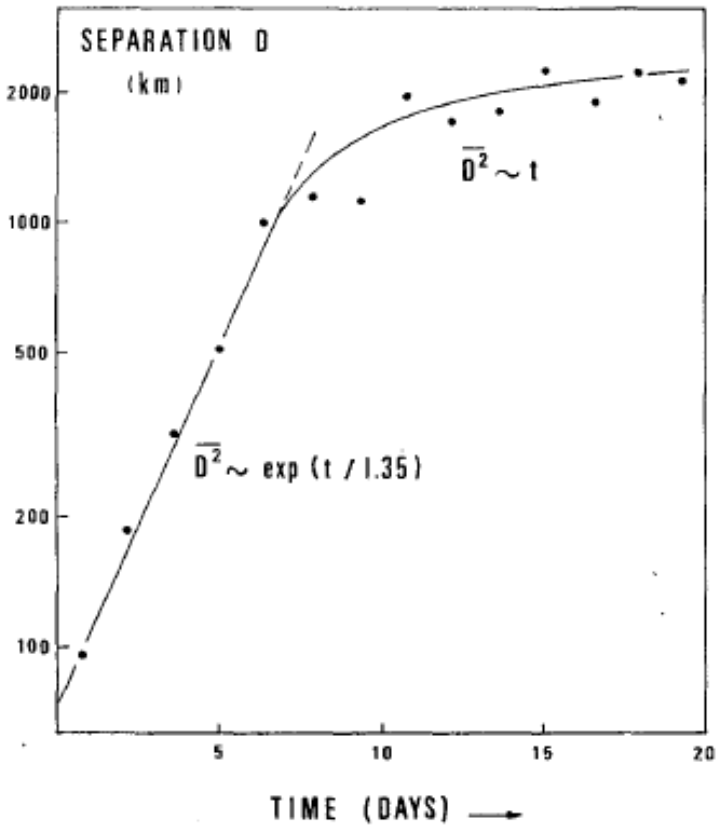

Figure 36: Relative dispersion for pairs of balloons from the EOLE experiment in the Southern Hemisphere. From Morel and Larcheveque (1974).

It is interesting to compare this with the Nastrom and Gage (1985) energy spectrum, in Fig. (22). There we saw evidence of a κ^{-3} spectrum at scales below roughly 2000 km. So the exponential growth seen here would be consistent. However, the energy spectrum also suggests a $\kappa^{-5/3}$ range at smaller scales. This would produce a t^3 growth in the dispersion, which we don't see. However, it's possible that is occurring below 100 km, the smallest scale sampled by the balloons. Er-El and Peskin (1981) examined another set of balloons, also from the Southern Hemisphere, and obtained

exponential growth at scales below 1000 km.

Two results from the ocean are shown in Fig. (37). Both involve surface buoys, deployed in the Gulf of Mexico during the SCULP experiment and in the Nordic Seas during the POLEWARD experiment. In both cases, we see indications of exponential spreading at the early times. In the Gulf, the growth occurs below scales of $\sqrt{2}2000 = 45$ km, and in the Nordic Seas it happens below the 10 km scale. In the Gulf case, the dispersion at large scales is super-diffusive. In the Nordic Seas case, the dispersion increases as t^3, up to 100 km, then grows diffusively thereafter. So it is possible there is an inverse cascade happening between 10-100 km in the eastern Nordic Seas.

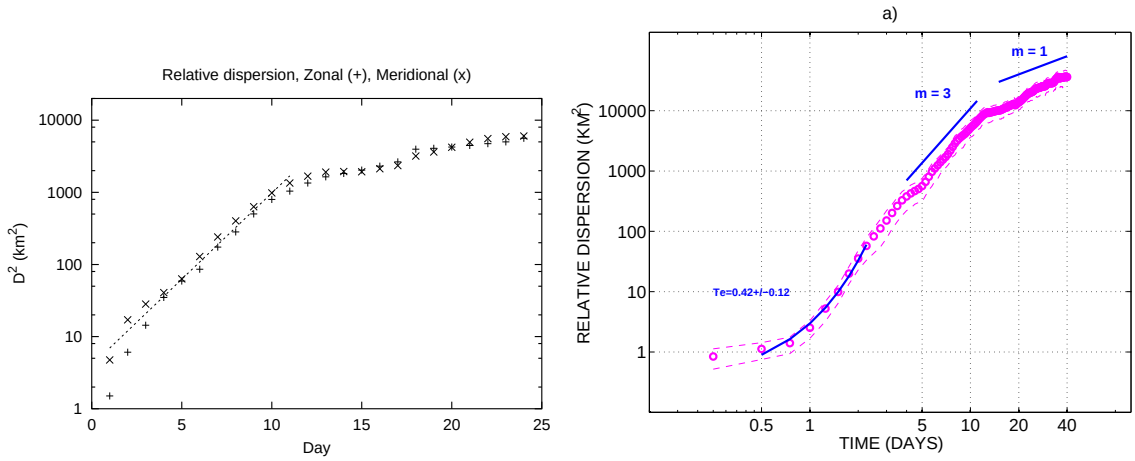

Figure 37: Relative dispersion for pairs of surface drifters in the Gulf of Mexico deployed during the SCULP experiment (left panel) and in the Nordic Seas during the POLEWARD campaign. Note the dispersion on the left is plotted on a semi-logarithmic plot and that on the right is on a logarithmic plot. From LaCasce and Ohlmann (1974) and Koszalka et al. (2009).

An interesting point is that 1000 km is comparable to the deformation radius in the atmosphere, and 45 km is similar to the deformation radius in the Gulf of Mexico. So both of these studies suggest exponential growth below the deformation radius. This is what one would expect if baroclinic

instability were causing a transfer of energy and enstrophy to the deformation radius, and if enstrophy were cascading to smaller scales.

Following Richardson (1926), one can write an equation for the probability of pair separations. It is possible to solve this equation and then compare the predicted probabilities with the observed distributions of pair separations for balloons or drifters. The details can be found in LaCasce (2010).